Multifunctional Magnetic Nanoparticles for Biomedical Applications

A Thesis Submitted towards Partial Fulfillment of

BS-MS Dual Degree Programme

By

Pravarthana Dhanapal

Under the Guidance of

Prof. S.B Ogale, NCL Pune, India

And

Dr. Seema Verma, IISER Pune, India

Department of Chemistry

Indian Institute of Science Education and Research (IISER) Pune

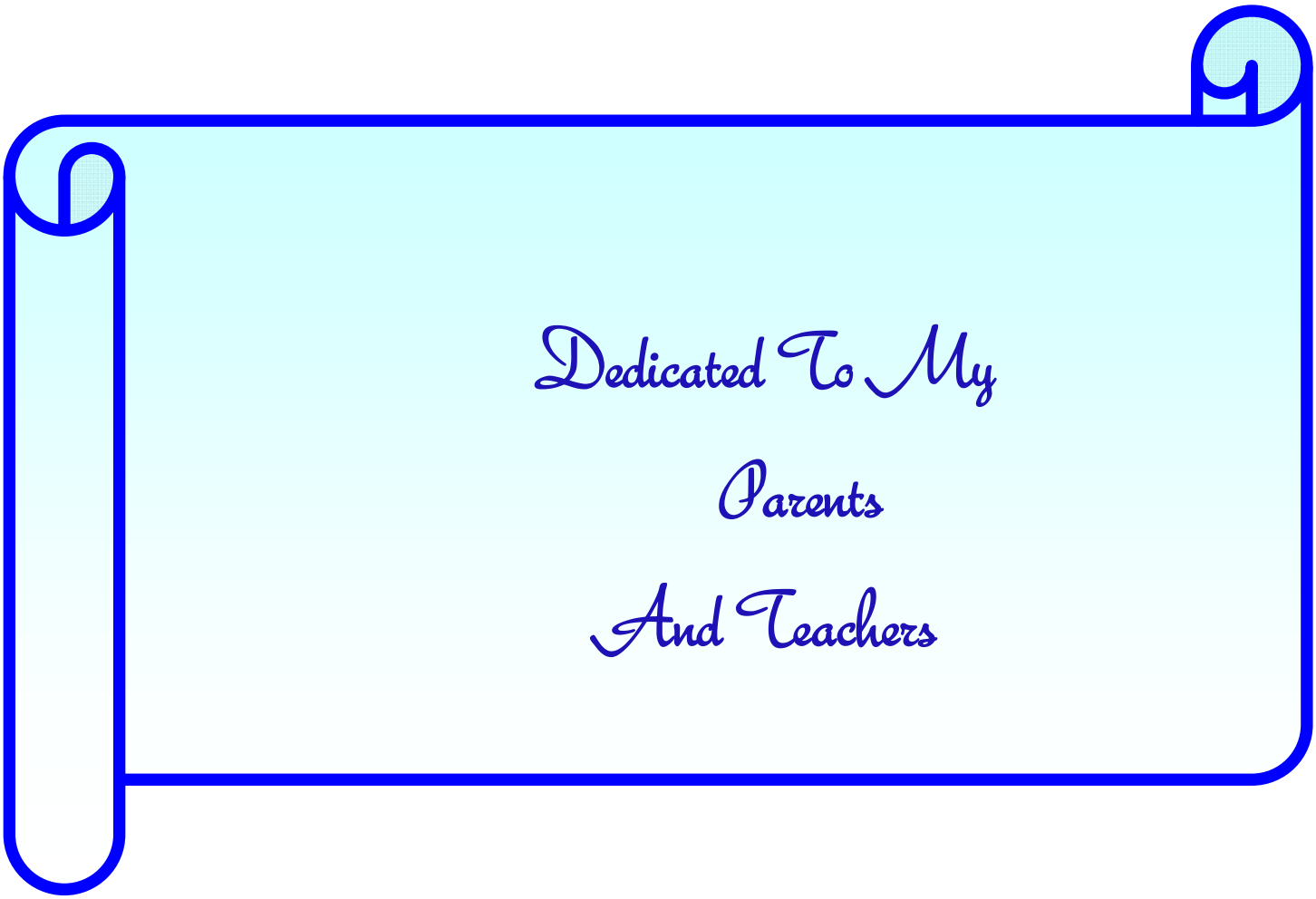
Dedicated To My
Parents
And Teachers

Contents

Certificate

This is to certify that this dissertation entitled "**Multifunctional Magnetic Nanoparticles for Biomedical Applications**" towards the partial fulfillment of the BS-MS dual degree programme at the Indian Institute of Science Education and Research Pune, represents original research carried out by **Pravarthana Dhanapal** at NCL and IISER Pune under the supervision of **Prof. S.B. Ogale**, NCL, pune and **Dr. Seema Verma,** IISER, Pune during the academic year 2010-2011.

Pravarthana Dhanapal

Prof. S.B Ogale
(Supervisor)
Date:
Place:

Dr. Seema Verma
(Supervisor)
Date:
Place:

Prof. K.N. Ganesh
Head (Chemistry)
Date:
Place:

Declaration by the Candidate

I declare that the thesis entitled "**Multifunctional Magnetic Nanoparticles for Biomedical Applications**" submitted by me for the degree of Master of Science for the record of work carried out by me during the academic year 2010-2011 under the guidance of **Prof. S.B Ogale**, NCL Pune and **Dr. Seema Verma**, IISER Pune. This work has not formed the basis for the award of any degree, diploma, and fellowship, titles in this or any other University or other institution of higher learning.

I further declare that the material obtained from other sources has been duly acknowledged in the thesis.

PRAVARTHANA DHANAPAL

DATE: 15th APRIL, 2011
PLACE: PUNE

Acknowledgements

I would like to express my deep sense of gratitude to Prof. S.B Ogale and Dr. Seema Verma for giving me an opportunity to pursue master's project with them. I am always indebted for their scientific advice, trust, continuous support, and co-operation during the course of this work.

I would like to thank all my labmates and friends Tushar, Vivek, Subas, Prasad, Abhimanyu, Meenal, Onkar, Reshma, Shruti, Vishal, Lily, Mandakini, Datta, Rohan, Abhik, Shraddha, Pradeep, Pooja, Satish, Ashish, Haribhau, Anil, Anirudh, Dr. Parvez Shaikh, Dr. Sarika Phadke, Keerthi for providing an academically exciting atmosphere. I would like to also thank other labmates Mangesh and Pankaj for their friendly interactions and support.

I wish to acknowledge all my teachers from primary schools to master's level who educated and nurtured me academically to reach at this destiny.

I take this opportunity to thank my beloved family members for their support, dedication and love. It gives me a great pleasure to acknowledge all those people whose help, wishes, encouragement and support have brought this task to its completion.

--- **Pravarthana Dhanapal**

List of Tables and Illustrations

List of Tables:-

List of Illustrations:-

List of Abbreviations

AFM	Atomic Force Microscopy
APTES	3-Amino propyl Triethyl silicate
CB	Conduction Band
CNTs	Carbon nanotubes
CTAB	Cetyl trimethylammonium bromide
DLS	Dynamic Light Scattering
DRS	Diffuse Reflectance Spectroscopy
EDC	Ethyl-3-[3-dimethylaminopropyl] carbodiimide Hydrochloride
FITC	Fluorescein isothiocyanate
HRTEM	High Resolution Tramission Electron Microscope
IBM	International Business Machines
JCPDS	Joint Committee for Powder Diffraction Standards
MRI	Magnetic Resonance Imaging
NHS	N-hydroxysuccinimide
NMP	N-methyl Pyrrolidone
NPs	Nanoparticles
PEG	Polyethylene glycol
PL	Photo-luminescence
QDs	Quantum Dots
SAED	Selected Area Electron Diffraction
TGA	Thermo-gravimetry Analysis
TEM	Transmission Electron Microscope
UV-VIS	Ultraviolet-Visible
XPS	X-ray Photoelectron
XRD	X-ray Diffraction
V B	Valence Band
VSM	Vibrating Sample Magnetometer
ZFC-FC	Zero Field Cooled-Field Cooled

Abstract

This thesis at the start of the chapter gives short introduction to the field of nanoscience. We have presented though brief but a critical review of literature on magnetic nanoparticles for biomedical application. Besides this, we have stated the objective and motivation behind this work and discussion of work in the subsequent chapters. The second chapter presents a brief description of various wet chemical synthetic routes, used for obtaining monodispersed nanoparticles. Brief discussions on various experimental tools were employed to characterize the synthesized nanoparticles for structural, optical and magnetic properties. In the final chapter we present a simple strategy to achieve nearly monodispersed γ-Fe_2O_3 nanoparticles by a thermal decomposition method utilizing a strong polar organic solvent, at much lower temperature of 200^oC. We demonstrate a generic approach to form stable dispersions of magnetic nanoparticles in both aqueous and non-aqueous media by appropriate surface functionalities. The amine functionalized magnetic nanoparticles enable the covalent conjugation of a fluorescent dye, which facilitates the use of these magnetic nanoparticles in biomedical applications.

CHAPTER I

INTRODUCTION

This chapter at the start gives short introduction to the field of nanoscience. We have presented though brief but a critical review of literature on magnetic nanoparticles for biomedical applications. Besides this, we have stated the objective and motivation behind this work and discussion of work in the subsequent chapters.

1 INTRODUCTION

Materials have been playing an extremely important role in the progress of human civilization since last many centuries. [1] Over the last 30 years, the synthesis of nanocrystals-crystalline particles ranging in size from 1 to 100 nm- has been intensively pursued, not only for their fundamental scientific interest, but also for their many technological applications. [2]Two principal factors decide the properties of nanoparticles (NPs) to differ significantly from bulk materials: increased surface to volume ratio and dominance of quantum effects. These factors can tune chemical reactivity, electronic, optical, mechanical, magnetic, and transport characteristics including properties such as ionization potential, electron affinity, capillary forces, melting point, specific heat etc. Here our objective seeks to understand these novel and interesting properties particularly by magnetic nanoparticles and explore them for biomedical applications.

1.1 Magnetic Nanoparticles

Magnetic materials have always attracted the attention of both scientists and technologist's because of the fascinating physical phenomena associated with them as well as their significance for several diverse and important application sectors. With the advent of nanotechnology the research on magnetic nanomaterials has intensified during the past decade and the emergent scientific activity promises major breakthroughs and developments in the fields of modern technology and biomedical applications. Biomedicine, targeted drug delivery, magnetic hyperthermia, MRI has become key areas of research harnessing the various unique properties of nanomaterials. Currently, magnetic nanoparticles are of great interest for researchers from a wide range of disciplines, including magnetic fluids,[3] catalysis,[4,5] biotechnology/biomedicine,[6] magnetic resonance imaging,[7,8] data storage,[9] and environmental remediation.[10a,11b] The combination of nanotechnology and molecular biology has developed into an emerging research area: nanobiotechnology.

Magnetism in solids arise from the magnetic ions or atoms distributed throughout a regular crystalline lattice on equivalent sites. The cooperative magnetism in solids is more complex than that of the isolated atoms because of the interaction (coupling) between the atomic moments. The essence of paramagnetism lies in the criterion that there is hardly any interaction between the individual magnetic moments in a long

range ordered crystalline lattice. In order to achieve the saturation magnetization of a paramagnet, where all the moments align parallel to the direction of the applied field, very high magnetic fields are required, simultaneously with very low temperatures. Ferromagnetic, ferrimagnetic and antiferromagnetic materials exhibit long-range ordering of the moments in the lattice. For ferro- and ferrimagnetic substances, the field dependence of magnetization is nonlinear and at large values of H, the magnetization M becomes constant at its saturation value Ms, as shown in Figure 1.1 But once saturated, a decrease in H to zero does not reduce M to zero. Hence it possesses some magnetization called remnant magnetization (M_R). In order to demagnetize the substance after saturation, a reverse field is required. The magnitude of this field is called coercivity (Hc). The M-H curve in the case of ferro- and ferrimagnets is called the magnetic hysteresis loop. In large particles, energetic considerations favor the formation of magnetic domains – groups of spins all pointing in the same direction and acting cooperatively – which are separated by domain walls with a characteristic width. In the case of these multidomain ferromagnetic particles, magnetization reversal occurs through the nucleation and motion of these walls. Fine particle magnetism has been traditionally dealt with the size effect, which is based on the magnetic domain structure of the magnetic materials [12a-f]. It assumes that the state of lowest free energy of ferromagnetic particles has uniform magnetization for the particles less than a certain critical size (single domain particles) and non uniform magnetization for the particles larger than the critical size (multi domain particles). As the particle size decreases toward some critical particle diameter, the formation of domain walls becomes energetically unfavorable and the particles are called single domain. Changes in the magnetization can no longer occur through domain wall motion and instead require the coherent rotation of spins, resulting in large coercivities. Nanosized magnetic materials exhibit a behavior similar to paramagnetism at temperatures below the Curie or the Neel temperature. It is half-way between ferro- and paramagnetism. In this case, below the Curie or Neel temperature, the thermal energy is not sufficient to overcome the coupling forces between neighboring atoms, whereas the energy is sufficient to change the direction of the magnetization of the entire particle. The resulting fluctuations in the direction of magnetization cause the magnetic moments average to zero. Thus, the material behaves in a manner similar to paramagnetism, except that instead of each individual atom being independently influenced by an external magnetic field, the

magnetic moment of the entire particle tends to align with the magnetic field. Thus, these particles are called superparamagnetic particles. Superparamagnetism occurs when the material is composed of very small crystallites. Experimental investigations on the dependence of the coercivity on particle size shows behavior similar to that schematically illustrated in Figure 1.2.

Superparamagnetism is a unique and important feature of magnetism in the nanosized particles. [13a-e] Superparamagnetic particles are ferro/ferri magnetic single domain particles, so small that thermal energy at that temperature of the experiment is of the same order or smaller than the energy barrier, preventing spontaneous reversal of magnetization. Thus, in a period comparable to the time of the experiment, the thermal energy equilibrates the magnetization of an assembly of such particles and the average magnetization is zero. For magnetic nanoparticles with spherical shapes, the magnetocrystalline anisotropy energy E_A can be approximated as the total magnetic anisotropy of single domain particles and can be expressed as $E_A = KV \, Sin^2\theta$, where K is the magnetocrystalline anisotropy constant, V is volume of a particle and θ is the angle between the direction of magnetization and the easy axis of magnetization. When E_A becomes comparable to thermal activation energy k_BT where k_B is the Boltzman constant, the magnetization direction starts flipping randomly and goes through rapid superparamagnetic relaxation. The temperature above which the thermal activation energy overcomes the magnetic anisotropy energy barrier and the nanoparticles become superparamagnetically relaxed is known as the superparamagnetic blocking temperature, T_B. Saturation magnetization of nanoparticle is also strongly dependent on their size. Intrinsically, magnetic materials possess magnetically disordered spin glass like layers near the surface due to the reduced spin-spin exchange coupling energy at the surface. [14e-f] In bulk cases, since the disordered surface layer is minimal compared with the total volume of the magnet, such surface spin canting effects are negligible. [14e]

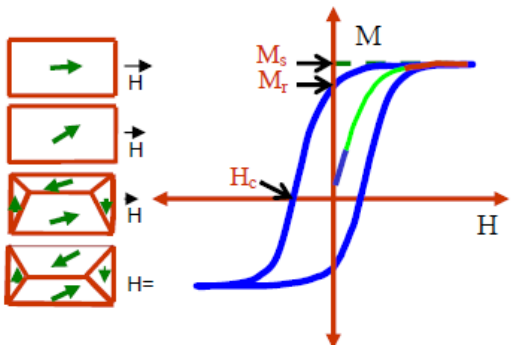

Figure 1.1 ***Magnetic domains and the process of magnetization in bulk magnetic materials***

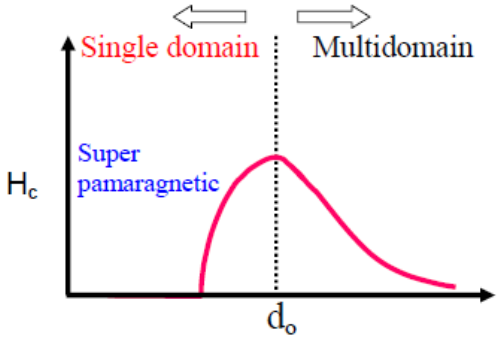

Figure 1.2. Particle size dependence Coercivity

Usually, superparamagnetic particles are characterized by a maximum in the temperature variation of ac susceptibility and zero-field-cooled (ZFC) susceptibility measured in a small dc magnetic field. [13f,g] The temperature at which a maximum is observed is the superparamagnetic blocking temperature T_B. When the same sample is cooled under a magnetic field (FC), the magnetization remains almost constant or deviates below the blocking temperature and overlaps with the ZFC magnetization, when the temperature rises above T_B. Such temperature dependence of the ZFC magnetization and the divergence of ZFC and FC magnetization below T_B are the characteristic features of superparamagnetism.

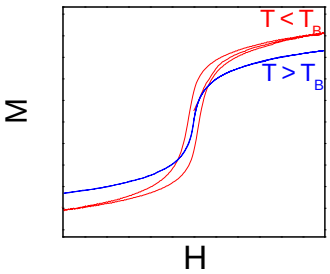

Figure 1.3 ***Typical FC and ZFC magnetization curves and field dependent magnetization behavior below and above the blocking temperature of superparamagnetic nanoparticles***

Opening up of the magnetic hysteresis loop is also expected below the blocking temperature. In magnetization measurements, superparamagnetic particles show a typical behavior as shown in figure 1.3. The characteristics of the FC magnetization curve depend on the nature of the interaction between the particles. If the particles are well separated in a non-magnetic matrix or by proper surface coatings, the different types of interactions between the particles such as dipolar interactions or exchange interactions are suppressed.

1.2 Biomedical Applications of Magnetic Nanoparticles

Magnetic nanoparticles are well-established nanomaterials that offer controlled size, ability to be manipulated externally, and enhancement of contrast in magnetic resonance imaging (MRI). As a result, these nanoparticles could have many applications in biology and medicine, including protein purification, drug delivery, and medical imaging. [15a]

Since magnetic nanoparticles can be easily conjugated with biologically important constituents such as DNA, peptides, and antibodies, it is possible to construct versatile nano-bio hybrid particles, which simultaneously posses magnetic and biological functions for biomedical diagnostics and therapeutics. Nanoscaling laws for magnetic components are found to be critical to the design of optimized magnetic characteristics of hybrid nanoparticles and their enhanced applicability in biomedical sciences including their utilizations as contrast enhancement agents for magnetic resonance imaging (MRI), ferromagnetic components for nano-bio hybrid structures, and translational vectors for magnetophoretic sensing of biological species. In particular, systematic modulation of saturation magnetization of nanoparticles probes is important to maximize MR contrast effects and magnetic separation of biological targets. [15b] Synthetic magnetic nanoparticles are emerging as versatile probes in biomedical applications, especially in the area of magnetic resonance imaging (MRI). Their size, which is comparable to biological functional units, and their unique magnetic properties allow their utilization as molecular imaging probes. [16] Magnetic cationic liposomes (MCLs), one of the groups of cationic magnetic particles, can be used as carriers to introduce magnetite nanoparticles into target cells since their positively charged surface interacts with the negatively charged cell surface; furthermore, they find applications to

hyperthermic treatments.[17]Magnetic nanoparticles that are superparamagnetic with high saturation moment have great potential for biomedical applications. Surface functinalization leads to the formation of water soluble nanoparticles that can be further modified with various biomolecules. Such functionalizations have shown promising applications in protein or DNA separation, detection and magnetic resonance imaging contrast enhancement. [18] Synthesis of multifunctional magnetic nanoparticles (MFMNPs) is one of the most active research areas in advanced materials. MFMNPs that have magnetic properties and other functionalities have been demonstrated to show great promise as multimodality imaging probes. Their multifunctional surfaces also allow rational conjugations of biological and drug molecules, making it possible to achieve target-specific diagnostics and therapeutics. [19]

1.3 Motivation behind the work

Monodisperse NPs with controlled shape and sizes are usually coated with a long chain hydrocarbon, leading to a hydrophobic surface. To make these NPs biocompatible for biological applications, their surfaces are often functionalized by means of surfactant addition or surfactant exchange. Surfactant addition is achieved through the adsorption of amphiphilic molecules that contain both a hydrophobic segment and a hydrophilic component. The hydrophobic segment forms a double layer structure with the original hydrocarbon chain, while hydrophilic groups are exposed to the outside of the NPs, rendering them water soluble. Surfactant exchange is the direct replacement of the original surfactant with a new bifunctional surfactant. This bifunctional surfactant has one functional group capable of binding to the NP surface tightly via a strong chemical bond and the second functional group at the other end has a polar character so that the NPs can be dispersed in water or be further functionalized. [30] Motivation behind the work is to accomplish optimal characteristic of multifunctional magnetic nanoparticle for biomedical application in a simplified way particularly small size (<50nm), excellent aqueous dispersity, high magnetic response (>10 emu/g) and to facilitate drug delivery, biosepartaion and bioimaging application. The task was organized by literature survey, finding out the chemical requirement for the work and finally targeting the synthesis towards pure phase, tunable size and shape, water soluble, biocompatible, and functionalizing with silica and Fluorescent molecule. We have successfully accomplished the work and discussed depth in the subsequent chapters.

1.4 REFERENCES

[1] (a) R.. E. Hummel, *Understanding of Materials Science*, 2nd Edition, Springer, **June 2004**. (b) K. J. Klabunde, *Nanoscale Materials in Chemistry*, A John Wiley and Sons Inc., Publication, **2001**. (c) M. Ratner, D. Ratner, *Nanotechnolgy*, Prentice Hall, **2002**.

[2] (a) G. Schmid, Nanoparticles: From Theory to Application, Wiley-VCH, Weinheim, 2004 (b) A.L Rogach, D.V. Talapin, E.V. Shevchenko, A. Kornowski, M. Haase, H.Weller, Adv. Funct. Mater. 2002,12, 653; (c) J.H. Fendler, Nanoparticles and Nanostructured Films, Wiley-VCH, Weinheim, 1988; (d) T. Hyeon, Chem. Commun.2003,927.

[3] S. Chikazumi, S. Taketomi, M. Ukita, M. Mizukami, H. Miyajima, M. Setogawa, Y. Kurihara, J. Magn. Magn. Mater 1987, 65, 245

[4] A.-H. Lu, W. Schmidt, N. Matoussevitch, H. Bonnermann, B. Spliethoff, B. Tesche, E. Bill, W. Kiefer, F. Schuth, Angew. Chem. 2004, 116,4403; Angew Chem. Int. Ed. 2004, 43, 4303.

[5] S. C. Tsang, V. Caps, I. Paraskevas, D. Chadwick, D. Thompsett, Angew. Chem. 2004,116,5763; Angew Chem. Int Ed. 2004,43,5645.

[6] A. K. Gupta, M. Gupta, Biomaterials 2005,26,3995.

[7] S. Mornet, S. Vasseur, F. Grasset, P. Verveka, G. Goglio, A. Demourgues, J. Portier, E Pollert, E. Duguet, Prog. Solid State Chem. 2006, 34, 237.

[8] Z. Li, L. Wei, M. Y. Gao, H. Lei, Adv. Mater. 2005, 17, 1001.

[9] T. Hyeon, Chem Commun. 2003, 927.

[10] (a) D. W. Elliott, W.-X. Zhang, Environ. Sci Technol. 2001, 35, 4922. (b) M. Takafuji, S. Ide, H. Ihara, Z. Xu, Chem. Mater. 2004, 16, 1977.

[11] (a) C. P. Bean and J. D. Livingston, Superparamagnetism, J. Appl. Phys. 30 (1959) S120-S129. (b) I. S. Jacobs, C. P. Bean, Magnetism, Ed. by G. T. Rado and H. Suhl, Academic Press, New York, 1963, vol. III. (c) E. P. Wohlfarth, Magnetism, Ed. by G. T. Rado and H. Suhl, Academic Press, New York, 1963, vol. III, 351. (d) B. D. Cullity, Introduction to Magnetic Materials, Addison Wesely, Reading MA, 1972. (e) Magnetic Properties of Fine Particles, Ed. by J. L. Dormann and D. Fiorani, North Holland, Amsterdam, 1992. (f) R. H. Kodama, Magnetic nanoparticles, J. Magn. Magn. Mater. 200 (1999) 359-372.

[13] (a) B. D. Cullity, Introduction to Magnetic Materials, Addison Wesely, Reading MA, 1972. (b) J. L. Dormann, D. Fiorani, and E. Tronc, Magnetic relaxation in fine particle systems, Adv. Chem. Phys. 98 (1997) 283-494. (c) W. F. Brown, Thermal fluctuations of a single domain particle, Phys. Rev. 130 (1963) 1677-1686. (d) Magnetic Properties of Fine Particles, Ed. by J. L. Dormann and D. Fiorani, North Holland, Amsterdam, 1992. (e) J. L. Dormann, D. Fiorani, and E. Tronc, Magnetic relaxation in fine particle systems, Adv. Chem. Phys. 98 (1997) 283-494. (f) Magnetic Properties of Fine Particles, Ed. by J. L. Dormann and D. Fiorani, North Holland, Amsterdam, 1992. (g) J. L. Dormann, D. Fiorani, and E. Tronc, Magnetic relaxation in fine particle systems, Adv. Chem. Phys. 98 (1997) 283-494.

[14] (a) C. Ellert, M. Schmidt, C. Schmitt, T. Reiners, H. Haberland, Phys. Rev. Lett. 1995, 75, 1731. (b) Jales, D Introduction to Magnetism and Magnetic Materials; CRC Press, Boca Raton, FL, 1998. (c) Cheon, J.;Kang, N.-J;Lee, S.-M.; Yoon, J.-H.; Oh, S.J. J. Am. Chem. Soc. 2004, 126, 1950-1951. (d) Park, J.; Kang, N.-J; Jun, Y.; Oh, S.J.; Ri, H.C.; Cheon, J. ChemPhysChem 2002, 3, 543-547. (e) Morales, M.P.; Veintemillas-Verdaguer, S.; Montero, M.I.; Serna, C.J. Chem. Mater. 1999, 11, 3058-3064. (f) Morales, M.P.; Serna, C.J.; Bodker, F.; Morup, S. J. Phys.: Conden. Matter 1997, 9, 5461-5467.

[15] (a) Jinhao Gao, Hongwei Gu, And Bing Xu, Accounts of Chemical Research 2009, 42, 1097-1107. (b) Young-Wook Jun, Jung-Wook Seo, and Jinwoo Cheon, Accounts of Chemical Research 2008, 41, 179-189

[16] Young-Wook Jun, Jae-Hyun Lee, and Jinwoo Cheon, Angew. Chem. Int. Ed. 2008, 47, 5122-5135.

[17] Akira Ito, Masashige Shinkai, Hiroyuki Honda and Takeshi Kobayashi, Journal of Bioscience and Bioengineering 2005, 100, 1-11.

[18] Chenjie Xu and Shouheng Sun , Polym Int 2007, 56, 821-826.

[19] Rui Hao, Ruijun Xing, Zhichuan Xu, Yanglong Hou, Song Gao and Shouheng Sun, Adv.Mater. 2010, XX, 1-14.

CHAPTER II

Synthesis and Characterizations Techniques

This chapter presents a brief description of various wet chemical synthetic routes, used for obtaining monodispersed magnetic nanoparticles. Various experimental tools employed to characterize the structural, optical and magnetic properties of the nanoparticles are discussed in the present chapter.

SECTION I: SYNTHESIS OF MONODISPERSED MAGNETIC NANOPARTICLES

In order to exploit the full potential of the synthesized nanoparticles, it is stringent requirement that they must be of same size and shape due to their strong size and shape dependence. Thus, to produce NPs of same size, shape, phase etc.; it will be worth for us to understand the actual NPs formation kinetics and their synthesis mechanism.

The NPs synthesis process basically consists of a nucleation step followed by particle growth stages.[1b] The solution must be supersaturated for nucleation to occur to form NPs. Supersaturation can be achieved either by directly dissolving the solute at higher temperature and then cooling to low temperatures or by adding the necessary reactants during the reaction.[1a] Generally, there are three kinds of nucleation processes viz. homogeneous, heterogeneous and secondary nucleation. Homogeneous nucleation occurs in the absence of a solid interface by combining solute molecules to produce nuclei. It happens due to the driving force of the thermodynamics because the supersaturated solution is not stable in energy. The overall free energy change, ΔG, is the sum of the free energy due to the formation of a new volume and the free energy due to the new surface created. For spherical particles

$$\Delta G = -4/V\pi r^3 k_B T \ln(S) + 4\pi r^2 \gamma \quad \ldots\ldots. (1.1)$$

$$r^* = 2V\gamma/3k_B T \ln(S) \ldots\ldots\ldots\ldots\ldots\ldots (1.2)$$

Where, V is the molecular volume of the precipitated species, r is the radius of the nuclei, k_B is the Boltzmann constant, S is the saturation ratio, and γ is the surface free energy per unit surface area. When $S > 1$, ΔG has a positive maximum at a critical size, r*. This maximum free energy is the activation energy for nucleation. Nuclei larger than the critical size will further decrease their free energy for growth and form stable nuclei that grow to form bigger particles. The critical nuclei size r* can be obtained by setting $d\Delta G/dr = 0$. For a given value of S, all particles with $r > r^*$ will grow and all particles with $r < r^*$ will dissolve. When the concentration drops below the critical level, nucleation stops and the particles continue to grow by molecular addition until the equilibrium concentration of the precipitated species is reached. Uniformity of

the size distribution is achieved through a short nucleation period which induces single nucleation event prohibiting additional nucleation, there by separarting nucleation and growth processes. To get a short burst of nucleation, a high saturation ratio (S) is suitable illustrated well by equation (1.2). Since NPs have large surface area, thereby huge surface energy and thus, are not thermodynamically stable. To overcome these problems to get stable NPs, it is required to arrest these NPs during the reaction either by adding surface protecting reagents, such as organic ligands or inorganic capping materials,[1a] or by placing them in an inert environment such as an inorganic matrix or polymers.[1b, c] The NPs dispersions are stable if the interaction between the capping groups and the solvent is favorable, providing an energetic barrier to counteract the Vander-waals and magnetic (in case of magnetic materials) interactions between them.

The synthesis of multi-functional NPs under technological desirable low temperature conditions with controlled size, shape and pure phase remains a major task for the researchers. Soft chemistry routes represent the most attractive alternatives, because they allow good control from the molecular precursors to the final product at low processing temperatures, result in the formation of NPs with high purity and compositional homogeneity. The present research work is mainly on Thermal decomposition and solvothermal methods for synthesis of monodisperse multi-functional magnetic nanoparticles.

2-I.1 Thermal Decomposition Methods

The thermal decomposition reactions of organometallic compounds and metal-surfactant complexes were performed in hot surfactant solutions in the presence of surfactants to synthesize nanoparticles of various materials. Organic-phase synthetic methods have been widely used to synthesize nanoparticles because of their many advantages, such as the high crystallinity and monodispersity of the synthesized nanoparticles and their high dispersion ability in organic solvents.

Sun and Zeng synthesized monodispersed iron ferrite nanocrystals by a high-temperature solution phase reaction of iron acetylacetonate with 1,2-hexadecanediol in the presence of oleic acid and oleylamine.[2a] By using a similar synthetic procedure, Sun et al. synthesized monodisperse nanocrystals of $CoFe_2O_4$ and $MnFe_2O_4$ from a high temperature reaction of $[Fe(acac)_3]$ and $[Co(acac)_3]$ or $[Mn(acac)_3]$ with 1,2

hexadecanediol.[2b] The particle diameter was tuned from 33 to 20 nm by varying the reaction conditions or by seed mediated growth.

Organic-phase hot-injection synthetic methods based on fast nucleation in organic surfactants solutions often result in a size distribution with σ = 10%, and a size-selection process is required to obtain monodisperse nanoparticles with a size distribution below 5%. This size-sorting process involves the gradual addition of a hydrophilic solvent to the nanoparticles dispersion in a nonpolar solvent, which results in precipitation. The large nanoparticles first precipitate because of their strong van der Waals attraction. This size-selection process is very laborious and tedious. [2c]

We have successfully synthesized nearly monodispersed γ-Fe_2O_3 NPs with appropriate surface functionality results in the formation of both hydrophobic and hydrophilic NPs in one pot reaction using thermal decomposition method. This has been discussed in the next chapter.

2-I.2 SOLVOTHERMAL METHOD

Hydrothermal syntheses involve chemical reactions in water which acts occasionally as catalysts and component of solid phase at elevated temperature (>100°C) and pressure (~ few atmospheres) in a sealed or closed system/vessel and are a special type of chemical transport reaction that relies on liquid-phase transport of reactants to nucleate to formation of the desired product. The selected reaction temperature and the degree of fill, or the percent of the reaction vessel free volume that is filled with water at room temperature, determine the prevailing experimental pressure. When water is used as a solvent, the dielectric constant and viscosity are also important. These decrease with rising temperature and increase with rising pressure, the temperature effect predominating. Owing to the changes in the dielectric constant and viscosity of water, the increased temperature within a hydrothermal medium has a significant effect on the speciation, solubility, and transport of solids. Therefore, the hydration of solids and the hydrolysis and speciation of aqueous cations at elevated temperatures are important steps in this process. [3]

We have adopted new strategy of synthesis of monodisperse γ-Fe_2O_3 NPs using solvothermal route to obtain both hydrophobic and hydrophilic. This has not been the part of thesis as further characterization need to be done.

SECTION II: MATERIALS CHARACTERISATION TECHNIQUES

2-II.1 X-RAY DIFFRACTION

X-ray diffraction (XRD) technique is used to realize structural properties of materials and get information like crystal structure/phase, lattice parameters, crystallite size, orientation of single crystals, preferred orientation of polycrystals, defects, strains and so on.[4] This technique is suitable for thin films, bulk and nanomaterials. In case of nanostructures, the change in lattice parameter w. r. t. bulk gives idea of nature of strain present in the film. In XRD, a collimated monochromatic beam of X-rays is incident on the sample for diffraction to occur. A constructive interference occurs only for certain θ's correlating to those (hkl) plane, where path difference is an integral multiple (n) of wavelength. Based on this, the Bragg's condition is given by

$$2d\sin\theta = n\lambda$$

Where, λ is the wavelength of the incident X-ray, d is the interplaner distance, 'θ' is the scattering angle and n is an integer-called order of diffraction.

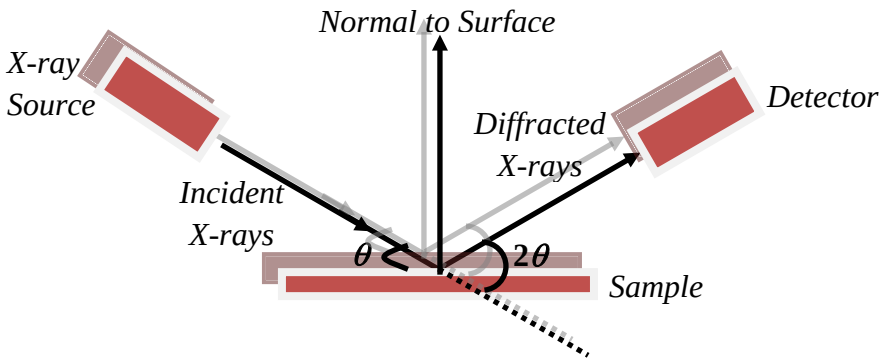

Fig. 2.1: **Representation of X-ray Diffraction**

The θ-2θ scan maintains these anglesThe samples were characterized for their phase purity and crystallinity by X-ray powder diffractometry (XRD) was carried out at room temperature (RT), using a model D8 ADVANCE BRUKER diffractometer wererecorded at IISER Pune equipped with Ni-filtered CuK_α radiation (λ = 1.5418Å, 40 kV and 30 mA). For identification purposes, the diffraction patterns obtained (I/I_o vs. *d*-spacing) were matched with JCPDS standards. Crystallite size was calculated using Scherrer formula in the framework of the X-ray line broadening technique.[4c]

2-II.2 MICROSCOPY TOOLS: during the course of research, we mainly used TEM and HRTEM for characterization of materials.

2-II.2a Transmission Electron Microscopy (TEM)

It is used to investigate the internal structure of nanomaterial. It works by passing electrons through the sample and using magnetic lenses to focus the image of the structure, much like light is transmitted through materials in conventional light microscopes. Because the wavelength of the electrons is much shorter than that of light, much higher spatial resolution is attainable for TEM images than for a light microscope. TEM can reveal the finest details of internal structure, in some cases individual atoms. TEM not only produces images but also electron diffraction patterns where high energy electron interacts with the sample which enables to make crystal structure analysis.

2-II.2b High resolution Transmission Electron Microscopy (HRTEM)

High-resolution transmission electron microscopy (HRTEM) is an imaging mode of the transmission electron microscope (TEM) that allows the imaging of the crystallographic structure of a sample at an atomic scale. Because of its high resolution, it is an invaluable tool to study nanoscale properties of crystalline material such as semiconductors and metals. Particle sizes were investigated by Transmission electron microscopy (TEM), high-resolution transmission electron microscopy (HRTEM) and selected area electron diffractometry (SAED) were performed on a FEI Technai 30 system microscope operated at 300 kV and 119 μA, on a carbon coated copper grid after dispersing nanoparticle on suitable solvent.

2-II.3 SPECTROSCOPY TOOLS

These tools are extremely sensitive to the aspects of electronic structure of the materials.

2-II.3a UV-VIS Spectroscopy

UV-VIS Spectroscopy deals with the recording of absorption signals due to electronic transitions. In semiconductors, when the incident photon energy exceeds the band gap energy of the materials, absorption takes place and signal is recorded by the spectrometer whereas in metals when the surface free electrons vibrate coherently with the incident frequency then resonant absorption takes place.

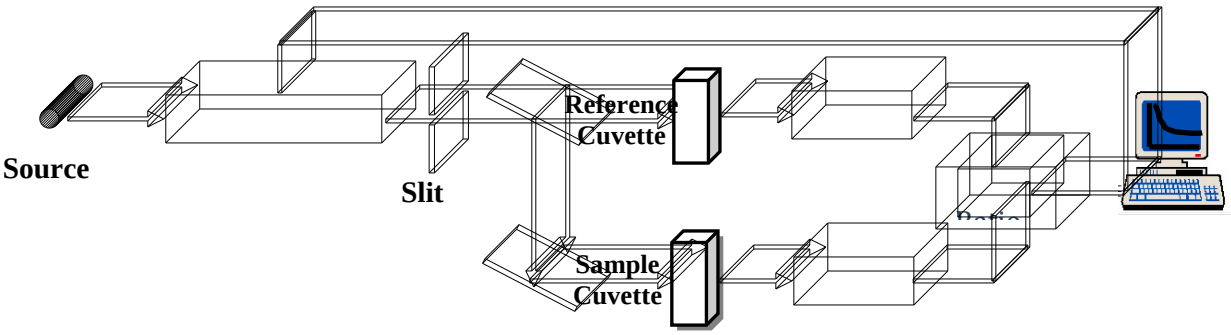

Fig. 2.2: Schematics of UV-VIS Spectrophotometer in Transmission Mode

This spectrometer can operate in two modes (i) transmission and (ii) reflection mode. In transmission mode usually thin films and colloidal NPs well-dispersed in solvent are used. The optical measurements for opaque thin films and those NPs which are not dispersible in solvents are done in diffuse reflectance (DRS) mode. UV-Vis diffuse reflectance spectroscopy (DRS) was carried out by means of a model 2100 UV-Vis Shimadzu spectrophotometer equipped with a diffuse reflectance attachment and a data acquisition system. Spectra were taken, over the wavelength range 200-800 nm, circular compacts of test materials against a $BaSO_4$ compact (a product of Shimadzu Corp.) used as a totally reflective reference material.In the present study measurements were carried out in National Chemical Laboratory, Pune, INDIA.

2-II.3b Fourier Transform IR Spectroscopy

IR spectrum appears only when the vibrations amongst bonded atoms produces a change in the permanent electric dipole moment of the molecule/solid. It is reasonable to suppose that the more polar a bond, the more intense will be IR spectrum arising from the vibrations of that bond. [5a,6] FTIR has considerably speeded and improved the spectroscopy in the IR region in general and in particular far IR region i.e. below 400 cm^{-1} where good deals of useful molecular information is contained, is usually called as 'Energy Limited' region, where sources become weak and detectors insensitive, resulting poor signal to noise ratio.

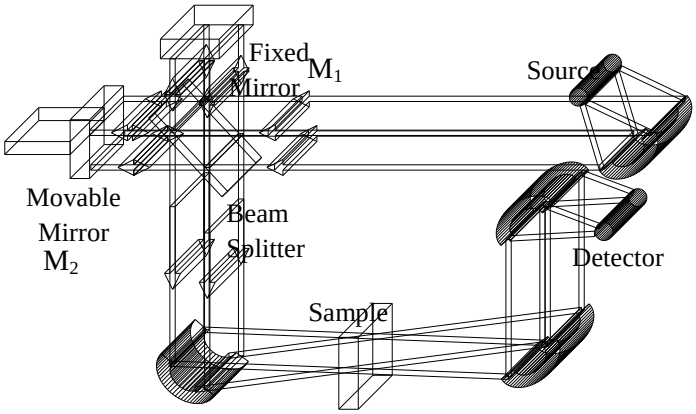

Fig. 2.3: **Schematic of FTIR Spectrophotometer**

Fourier transform infrared spectra (FTIR) of the pure liquid of oleic acid, oleylamine and the equimolar mixture of oleic acid and oleylamine were obtained by drop casting the liquids dissolved in chloroform onto the NaCl window allowing the solvent to evaporate. The transmission FTIR spectra of magnetic nanoparticles were recorded in the 400-4000 cm^{-1} range (Nicolet 6700) by preparing KBr (Sigma Aldrich, spectroscopy grade) pellets (0.1 wt% sample).The FTIR measurements of these samples were carried out on a Nicolet 6700 FTIR spectrometer at IISER, Pune, INDIA.

2-II.3c Photoluminescence Spectroscopy

Photoluminescence (PL) is the spontaneous emission of light from a material under optical excitation. The appropriate excitation energy and intensity is required to choose to probe the sample's discrete electronic states accurately. When light of

sufficient energy is incident on a material, photons are absorbed, material got excited and electronic transitions occurred. Eventually, these excitations relax and the electrons return to the ground state. If radiative relaxation occurs, the emitted light is called PL. This light can be collected and analyzed to yield a wealth of information about the photo-excited material. The PL spectrum provides the transition energies, which can be used to determine electronic energy levels, defects and impurity states in the sample. The PL intensity gives a measure of the relative rates of radiative and non-radiative recombination. [7,5b] The intensity of the PL signal depends on the rate of radiative and nonradiative events, which depends in turn on the density of nonradiative interface states.

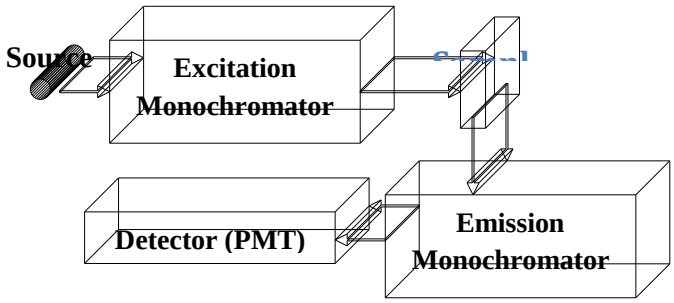

Fig. 2.4: Schematic Layout of PL Set-up

The PL measurements of nanopowders and NPs dispersed in solvent were done using LS 55 spectrophotometer at National Chemical Laboratory, Pune, INDIA.

2-II.3d X-ray Photoelectron Spectroscopy

X-ray photoelectron Spectroscopy (XPS) probes the binding energies of core electrons in an atom. Although such electrons play little part in chemical bonding, different chemical environments can induce small changes in their binding energies; this is because the formation of bonds; changes the distribution of electrons in the system and hence, by modifying nuclear shielding, produces changes in the effective nuclear charge of the bound atoms. Thus, XPS involves the analysis of emitted electrons from a material as a result of incident X-rays, is also rarely called as electron spectroscopy for chemical analysis (ESCA). Only the photoelectrons from atoms near the surface escape, typically from top 2-5 nm. The actual depth varies with the materials and electron energy. A typical sampling area is 1 cm^2.

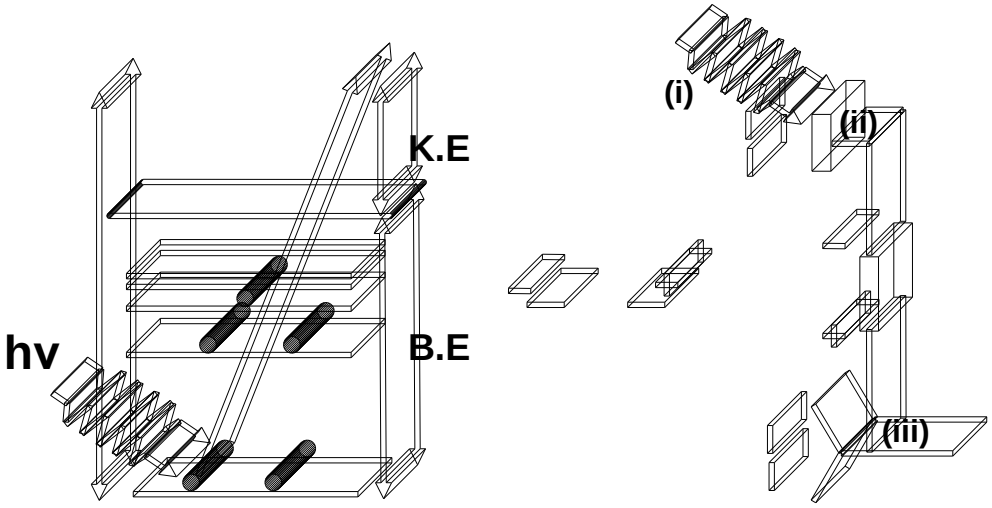

Fig. 2.5: (A) Principle of Photo-electron spectroscopy, (B) Schematic of XPS/UPS [5c]

This technique mainly gives information about the elemental composition of the surface of the materials and the information about the chemical state of elements. It is one of the most employed surface analysis techniques. This is usually performed using X-rays (typically from Al or Mg) to excite photoelectrons from the core levels of atoms in a specimen. [5] Powder samples drop casted to form a film and this film was used for the XPS measurements. The measurements were performed on VG microteck ESCA 3000 instrument at a pressure of 10^{-9} torr. The general scan, C_{1s}, O_{1s}, Ti_{2p} and Fe_{2p} were recorded with non-monochromatized MgK_{α} radiation with photon energy = 1253.6 eV with a pass energy of 50 eV and an electron take off angle of 55^{o}. The overall resolution for the XPS measurements was 0.2 eV. The core level spectra were background corrected using Shirley algorithm and the peak fittings were done using XPSPEAK 41 software. The core level binding energies were aligned with respect to C_{1s} binding energy of 285 eV. The measurement was carried out in Center for Materials Characterizations (CMC), National Chemical Laboratory, Pune. The core level binding energies (BE) were corrected with the carbon binding energy of 285 eV.

2-II.3e Vibrating Sample Magnetometer (VSM)

VSM involves the measurement of magnetic induction in the vicinity of the sample [8]. According to Faraday's law of electromagnetic induction, an emf (V) will be generated in a coil when there is a change in Flux linked to coil. For a given coil, with *n* turns and cross-sectional area, *a*

$$V = -na\underline{dB/}dt \quad (1.4)$$

where *B*, magnetic induction is equal to the product of the constant applied Field, *H*, and the permeability, μ_0. But when a sample with magnetization *M* is introduced into the coil, the magnetic induction becomes;

$$B = \mu_0(H + M) \quad (1.5)$$

Incorporating the corresponding flux change, ¢$B = \mu_0 M$, into the Equation 1.4, the output signal of the coil is obtained as

$$V\,dt = -na\,\mu_0 M \quad (1.6)$$

That is the output signal is independent of the magnetic Field, *H*, in which the measurement has been carried out.

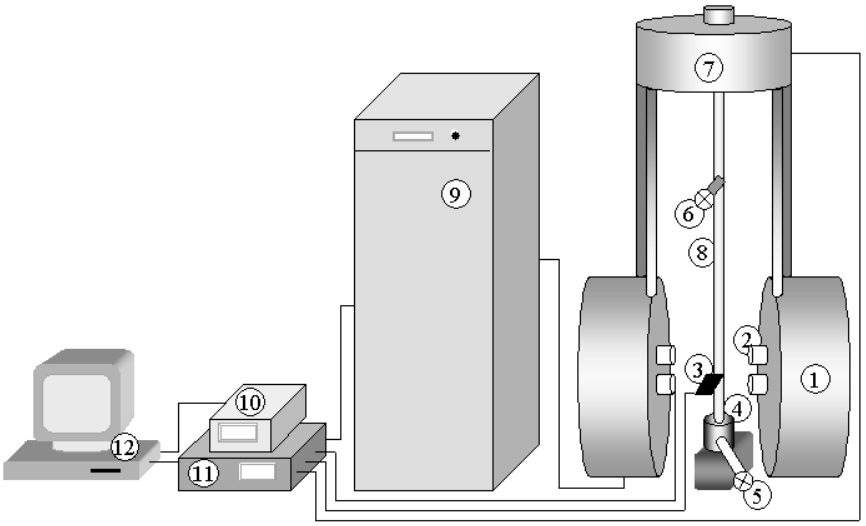

Figure 2.6: Schematic diagram of Vibrating Sample Magnetometer.

Vibrating Sample Magnetometer (VSM) measures the voltage induced by a sinusoidal motion of the sample, produced with the help of a transducer assembly, in vertical direction with respect to the magnetic field. The sample is centered in the region

between the magnetic poles and the stationary pick-up coils are suitably located on the magnetic pole pieces. Here, the frequency of the output signal is the same as the vibrational frequency of the sample, whereas, the intensity of the signal is determined by the magnetic moment as well as the frequency and amplitude of sample vibration. Therefore, in order to avoid any errors due to variations in the amplitude or frequency of vibration, usually a reference technique is employed. This is done by using a vibrating capacitor which generates a reference signal that is sensitive to the vibrational amplitude and frequency. A schematic diagram of the VSM is given in Figure 2.6. Magnetic measurements of the present work are performed on a PAR EG&G 4500 vibrating sample magnetometer. Calibration of this VSM is done by using a standard nickel sample which gives a saturation magnetization value of 490 emu/g, in a wide range of temperatures around room temperature. The sample holder used is made of a non-magnetic a polymeric material, Kel-F (poly(chlorotriflouro)ethylene). Field dependence of magnetization is done using a maximum magnetic field of $\pm$15000 Oe. The temperature range in which magnetic properties are studied is 10-873 K. Most of the measurements are carried out at 300 K . A closed cycle helium cryostat is used for measurements in the 10-300 K range and an oven assembly is used for measurements above room temperature. Temperature variation of magnetization is measured by two methods. The first one involves cooling the samples in zero magnetic field from room temperature to the lowest measuring temperature and then the magnetization is recorded while warming the sample in a lower field (generally 50 Oe). This method is called zero field cooled, ZFC, magnetization measurement. In the second method, the sample is cooled under an applied magnetic field itself and the magnetization is monitored while heating in the same field. This method is called the field cooled (FC) magnetization measurement. Zero field cooled (ZFC) magnetization measurements, using very low magnetic fields, are found to be useful for the identification of different magnetic phases coexisting in a given sample of R-site substituted manganates [9]. Therefore ZFC magnetization curves are recorded for all the samples at a lower field of 50 Oe. Curie temperature (T*c*) is determined as the temperature at which a maximum is observed in the *d*M/*d*T versus T curves.

2-II.3f Thermogravimetric Analysis

Thermogravimetry (TG) is the branch of thermal analysis which examines the weight change of a sample as a function of temperature in the scanning mode or as a function of time in the isothermal mode. In the present study, dynamic thermogravimetry technique is used, in which the sample is heated in an environment whose temperature is changing in a predetermined manner, at a linear rate. There are many events considered in TG, such as desorption, absorption, sublimation, vaporization, oxidation, reduction and decomposition. Moreover, TG is used to characterize the decomposition and thermal stability of materials under variety conditions [10, 11]. TG curves are usually recorded using a thermobalance.

A Perkin Elmer: STA 6000 thermal analyzer at IISER pune, India was used to perform the thermogravimetric analysis (TGA) of samples. Thermal analysis was carried out up to 1073K in flowing air, at a heating rate 10 K/min.

2-II.3g DYNAMIC LIGHT SCATTERING

Dynamic Light Scattering is also known as Photon Correlation Spectroscopy.This technique is one of the most popular methods used to determine the size of particles. Shining a monochromatic light beam, such as a laser, onto a solution with spherical particles in Brownian motion causes a Doppler Shift when the light hits the moving particle, changing the wavelength of the incoming light. This change is related to the size of the particle. It is possible to compute the sphere size distribution and give a description of the particle's motion in the medium, measuring the diffusion coefficient of the particle and using the autocorrelation function. This method has several advantages: first of all the experiment duration is short and it is almost all automatized so that for routine measurements an extensive experience is not required. Moreover, this method has modest development costs. Commercial "particle sizing" systems mostly operate at only one angle (90°) and use red light (675 nm). Usually in these systems the dependence on concentration is neglected. Using more sophisticated experimental equipment (projector, short wavelength light source), the methods can be not only considerably extended, but also more complicated and expensive.[12]

Although dynamic scattering is, in principle, capable of distinguishing whether a protein is a monomer or dimer, it is much less accurate for distinguishing small

oligomers than is classical light scattering or sedimentation velocity. The advantage of using dynamic scattering is the possibility to analyze samples containing broad distributions of species of widely differing molecular masses (e.g. a native protein and various sizes of aggregates), and to detect very small amounts of the higher mass species (<0.01% in many cases). Furthermore, one does not have to worry that protein aggregates are being lost within a chromatographic column (a common problem in using SEC to characterize aggregates), because there is no chromatographic separation involved. Moreover, with this technique it is also possible to obtain absolute measurements of several parameters of interest, like molecular weight, radius of gyration, Translational diffusion constant and so on. However, the analysis might be difficult for non-rigid macromolecules. Another limit is that above the zero degree Kelvin molecules fluctuate (i.e. molecules deviate from their average position).[13]

Zeta potential is widely used for quantification of the magnitude of the electrical charge at the double layer. In our work zeta potential of magnetic nanoparticle was calculated from DLS.Zeta potential measurement of the samples were carried out on a Dynamic light Scattering with zeta potential, Malvern zetasizer Nano ZS90 IISER, Pune, INDIA.

2-III REFERENCES

[1] (a) C. Burda, X. Chen, R. Narayanan, M.A. El-Sayed, *Chem. Rev.* **2005**, *105*, 1025; (b) X. Peng, J. Wickham, A. P. Alivisatos, *J. Am. Chem. Soc.* **1998**, *120*, 5343; (c) J. Park et.al., *Angew. Chem. Int. Ed.* **2007**, *46*, 4630

[2] (a) S. Sun, H. Zeng, J. Am. Chem. Soc. 2002, 124, 8204. (b) S. Sun H.Zeng, D.B Robinson, S.Raoux, P.M. Rice, S.X. Wang, G. Li, J. Am. Chem. Soc. 2004, 126, 273. (c) Jongnam Park, Jin Joo, Soon Gu Kwon, Youngjin Jang, and Taeghwan Hyeon Angew. Chem. Int. Ed. 2007, 46, 2-33

[3] S. Somia, R. Roy, *Bull. Mater. Sci.*, **2000**, *23*, 453.

[4] *(a) Elements of X-ray Diffraction*, ed. by B. D. Cullity (Addison Wesley Publishing Co., **1978**). (b) *Nanostructures and Nanomaterials: Synthesis, Properties and Applications, by G. Cao (Imperial College Press)*, **2004**. (c) H.P. Klug, L.E. Alexander, X-ray Diffraction Procedures for Polycrystalline and Amorphous Materials, 2nd edn., J. Wiley & Sons, New York, 1974, 618.

[5] (a) C. N. Banwell, E. M. McCash, A Book: *Fundamentals of Molecular Spectroscopy*, 4th Ed., Tata McGraw Hill Publishing Co. Ltd., **2002** (b) A Book: Nanotechnology, By S.K.Kulkarni, Capital Publishing Co., **2007**. (c) T. Wu, S. B. Ogale, J. E. Garrison, B. Nagaraj, A. Biswas, Z. Chen, R. L. Greene, R. Ramesh, T. Venkatesan, A. J. Millis, *Phys. Rev. Lett*., **2001,** *86*, 5998

[6] J. Coates, *Interpretation of Infrared Spectra: A Practical Approach*, *Encyclopedia of Analytical Chemistry*, R.A. Meyers (Ed.), *10815*, John Wiley & Sons Ltd, **2000**.

[7] T. H. Gfroerer, *Photoluminescence in Analysis of Surfaces and Interfaces*, *Encyclopedia of Analytical Chemistry*, R.A. Meyers (Ed.), 9209, John Wiley & Sons Ltd, Chichester, **2000**.

[8] Buschow, K. H. J., De Boer, F. R., in: *Physics of Magnetism and Magnetic Materials*, Kluwer Academic/Plenum Publishers, New York [2003].

[9] Anil, K. P. S., Alias, J. P.,Date, S. K., *J. Mater. Chem.* 8, 1219 [1998].

[10] W. WM. Wendlant, *Thermal Methods of Analysis*, 2nd ed. (John Wiley & Sons, New York, 1974).

[11] T. Hatakeyama, and F. X. Quinn, *Thermal Analysis: Fundamentals and Applications to Polymer Science*, (John Wiley & Sons, New York, 1995).

[12] Berne and Pecora, "Dynamic Light scattering" John Wiley, 1975

[13] American Journal of physics volume 38, number 5, may 1970, (pg 575-585)

CHAPTER III

Monodispersed γ-Fe_2O_3 Nanoparticles: Tunable Surface Functionalities for Biomedical Applications

Present study provides a simple strategy to achieve nearly monodispersed γ-Fe_2O_3 nanoparticles by a thermal decomposition method utilizing a strong polar organic solvent, at much lower temperature of 200^{o}C. We demonstrate a generic approach to form stable dispersions of magnetic nanoparticles in both aqueous and non-aqueous media by appropriate surface functionalities. The amine functionalized magnetic nanoparticles enable the covalent conjugation of a fluorescent dye, which facilitates the use of these magnetic nanoparticles in biomedical applications

SECTION I: One-Pot Synthesis of Monodispersed γ-Fe_2O_3 Nanoparticles

3-I.1 INTRODUCTION

With the advent of nanotechnology the research on magnetic nanoparticles has intensified during the past decade and the emergent scientific activity promises major breakthroughs and developments in the fields of modern technology and biomedical applications. Over the past few years magnetic nanoparticles (MNP) are attracting interest, mainly due to their promising applications in biomedicine and nonlinear optics.[1-3] As the size is reduced, the magnetic structure at the surface layer differs from that of the particle core, giving rise to remarkable effects on the magnetic ordering within the whole particle.[4,5] Consequently, understanding and controlling the effects of surface chemistry on the magnetic properties have become increasingly important issues for many technological applications of MNP, such as high density magnetic storage, magnetic resonance imaging, and drug delivery.

The use of MNP in biomedical applications may bring about significant advanced in diagnosis, prevention, and treatment of diseases.[6] The potential application of MNP for biomedical purposes relies on the synthesis of high quality materials, mainly regarding crystallinity and magnetic response. In this respect, it is essential to minimize the polydispersity and heterogeneity of the particles and to maximize their magnetic response. MNP for drug delivery and contrast agents for magnetic resonance imaging must exhibit a high magnetic response to external fields and should have functinalized, biocompatible surfaces.[7,8] However, the synthesis of such MNP is, in general, a critcal issue since the properties of each specific sample depend on several parameters in a complex manner. Deeper understanding of these complex effects is necessary to design and control new synthesis methods yielding high quality MNP. In this respect, some mechanisms have been recently reported that may enable the synthesis of such kind of particles.[9]

Syntheses based on the decomposition of organometallic precursors have proved successful for the preparation of monodispersed nanoparticles.[10-14] In particular, the synthesis of iron oxide nanoparticles (magnetite/maghemite Fe_3O_4 / γ-Fe_2O_3) by

thermal decomposition of an organic iron precursor in a high boiling point organic solvent yields highly crystalline MNP with excellent magnetic properties. [15,16]

In the present investigation, a much convenient polar organic solvent, N-methyl 2-pyrrolidone (NMP) has been introduced for the first time to synthesize highly monodispersed magnetic nanocrystals. This is particularly due to its stability at the ambient temperature, low flammability, low volatility and its ready availability with no clear toxicity profile. Importantly, the reaction has been carried out at comparatively much lower temperature of ~ 200ºC in the ordinary laboratory equipments. Although, this thermal decomposition method has become the main approach to achieve good quality highly monodispersed magnetic nanocrystals, the choice of the surfactants play an important role in enhancing the thermal and chemical stability of the nanoparticles. Fatty acid, especially oleic acid, $C_{17}H_{33}COOH$ (R-COOH) and olyelamine, $C_{18}H_{35}NH_2$ (R*-NH_2) is a commonly used surfactant to stabilize the magnetic nanocrystals in the organic phase.[17,18] However, a much used and well reported surfactant to synthesize chemically stable magnetic nanocrystals is the equimolar mixture of both oleylamine and oleic acid. [19] We investigate effect of concentration of oleic acid and olyelamine on size, shape and magnetic properties of γ-Fe_2O_3 nanoparticles. We have chosen equimolar mixture of both oleylamine and oleic acid for phase transfer as the particles are monodispersed and uniformly spherical shape. The work is in progress for further characterization of aqueous transfered γ-Fe_2O_3 nanoparticle. We present a simple strategy to obtain water soluble γ-Fe_2O_3 nanoparticles with surface functionalities utilizing Polyethylene glycol (PEG) of Mn 10,000, 3-Amino propyl Triethyl silicate (APTES) and 11-Aminodecanoic acid. We have further chosen amine functionalized γ-Fe_2O_3 nanoparticle to obtain fluorescent magnetic nanoparticle.

3-I.2 EXPERIMENTAL

The chemicals iron (III) acetylacetonate, Tetramethyl Ammonium Hydroxide (TMAOH), Cetyl trimethylammonium bromide (CTAB), Polyethylene glycol (Mn 10,000), 3-Amino propyl Triethyl silicate (APTES), Fluorescein isothiocyanate (FITC), 1-Ethyl-3-[3-dimethylaminopropyl] carbodiimide Hydrochloride (EDC), N-hydroxysuccinimide (NHS), Triethyl amine (TEA), 11-Aminodecanoic acid (11-AM), oleic acid (Oa), and oleylamine (Oam) were purchased from Aldrich Chemicals. N-metyl 2-pyrrolidone (NMP) was purchased from Merck Chemicals. All the Chemicals were of analytical grade or better. Iron acetylacetonate (0.1M), dissolved in 15 ml of NMP was taken in a pressure equalizer attached to a three neck round bottom (RB) flask. In RB flask, surfactants were mixed with 35ml NMP and magnetically stirred under a flow of argon. The mixture was heated to reflux at 200 ºC. To this solution, iron acetylacetonate solutions was injected instantaneously and was further refluxed for 1 hr. After one hour the heat source is removed and the black brown mixture was further stirred for ~ 18 hrs. The black material was precipitated after adding suitable solvent. The black product was centrifuged for 10 minutes with the speed 10,000 rpm. The This procedure of precipitation and centrifugation was repeated two to three times to remove the solvent and excess surfactants. The precipitate was dispered in suitable solvent and dried at 50 ºC in a vacuum oven for further chracterization. In order to investigate the effect of concetration of oleic acid and oleyl amine on size and shape of γ-Fe_2O_3 nanoparticles molar ratio of oleic acid and oleyl amine as indicated in Table 1 was varied to obtain (a) FeA, (b) FeB and (c) FeC.

3-I.3 RESULTS AND DISCUSSION

Figure 3.1 shows the representative TEM images of γ-Fe_2O_3 nanoparticles synthesized by different molar ratio of oleic acid and oleyl amine. Analysis of TEM micrographs clearly indicate the formation of monodispersed spherical nanoparticles for FeA. Whereas FeB and FeC show the formation of irregular shaped particles. Particle size distribution anaylsis shows narrow size distribution for FeA with mean particle size of 5 + 0.2 nm. On the other hand both FeB and FeC show wide particle size distribution. The lattic fringe analysis of FeA sample is included as the inset in figure 3.1 (a) with fringe analysis .

Table 3.1 Sample code, Molar ratio of Oa: Om, TEM particle size and XRD crystallite size

Sample Code	Molar ratio of Oa :Oam	TEM particle size (± 0.2nm)	XRD Crystallite size (± 0.5nm)
FeA	01:01	5	6
FeB	01:05	10	11
FeC	00:01	10	10

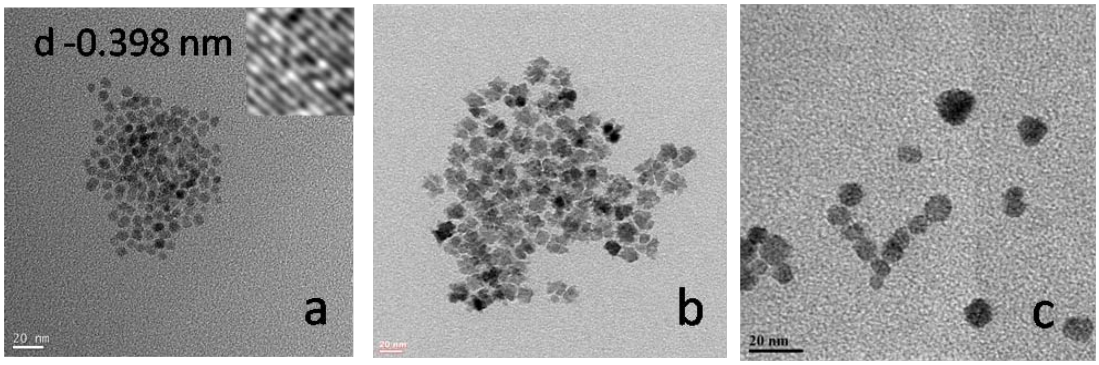

Figure 3.1: TEM images of for γ-Fe_2O_3 nanoparticles (a) FA , (b) FeB and (c) FeC. Inset (a) corresponds to lattice fringes from HRTEM analysis

Figure 3.2 show powder x-ray diffraction patterns of γ-Fe_2O_3 nanoparticles. The XRD peak positions and relative intensities matches well with the JCPDS standard [39-1346]. The average crystallite sizes were calculated using scherrer formula. XRD crystallite sizes and TEM particle sizes are shown in Tabale 1 for comparsion.

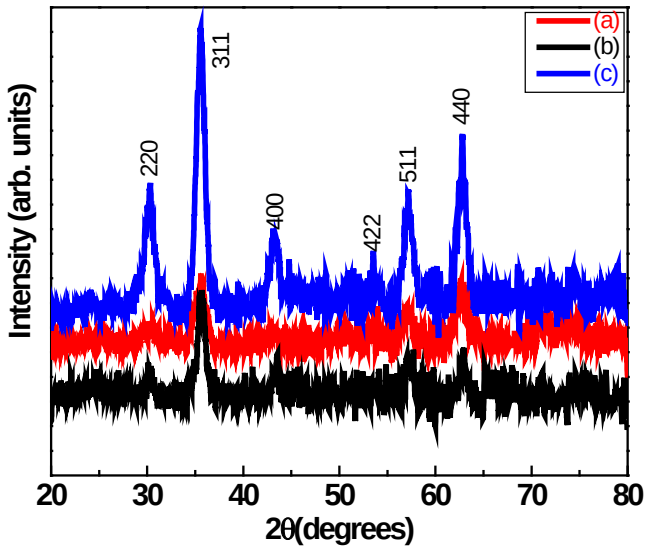

Figure 3.2: XRD patterns for γ-Fe_2O_3 nanoparticles (a) FeA,(b) FeB and (c) FeC

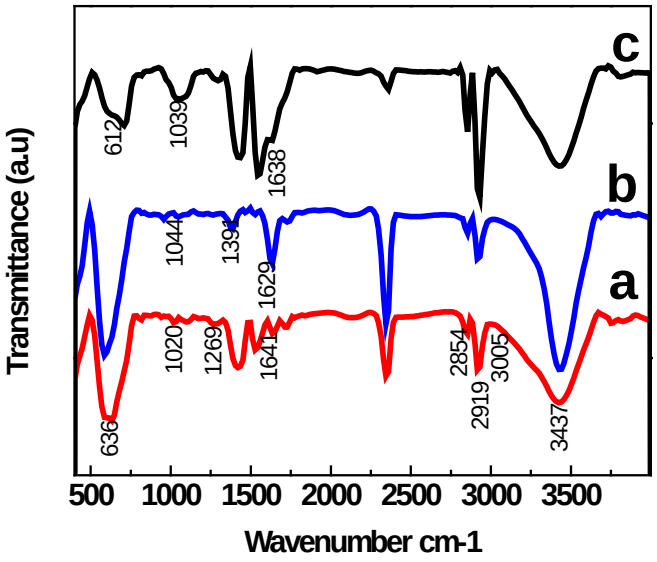

Figure 3.3: FTIR spectra of (a) FeA, (b) FeB, and (c) FeC

Figure 3.3 illustrates the FTIR spectra of the surfactant coated γ-Fe_2O_3 nanoparticles taken in 0.1wt% of the sample in KBr. No spectral features corresponding to free oleic acid (RCOOH) and free oleylamine (R*NH_2) is found in the FTIR spectra of γ-Fe_2O_3 nanoparticles (a) FeA and (b) FeB. Similarly free oleylamine (R*NH_2) is found in the FTIR spectra of γ-Fe_2O_3 nanoparticles with surfactant concentration (c) FeC. There is no shift in methylene asymmetric (v_{as} (CH_2) and symmetric (v_s (CH_2) (2919 cm^{-1}, 2854 cm^{-1}) stretching bands of in the

sample.A weak broad absorption peak around 1625 cm^{-1} could be attributed to that of the antisymmetric deformation of the NH_3^+ group which may display the presence of the protonated amines. [20] This band is superimposed to the broad peak at 1648 cm^{-1} suggesting that the C=C bond is intact in the oleyl groups on the surfactant. Importantly, absence of 1710 cm^{-1} band corresponding to C=O stretch bond of the carboxyl group (of pure oleic acid) and the appearance of two new bands characterstics of asymmetric (v_{as} (COO^-)) and (v_s (COO^-)) stretch at 1531 and 1427 cm^{-1} (curve a and b) γ-Fe_2O_3 nanoparticles confirm the formation of deprotonated carboxylate. Interestingly, there is no characterstic peak for oleylamine indicating bsence of NH_2 bond on the surface of the magnetic nanoparticles. [23] The characteristic spinel absorption bands at 636 cm^{-1} confirm the formation of γ-Fe_2O_3 nanoparticles. [24(a,b)] Hence it is observed that in γ-Fe_2O_3 nanoparticles (a) FeA and (b) FeB the mechanism of binding is with mixed oleic acid and oleylamine surfactants through protonation of amine and deprotonation of carboxylate group. In case of FeC the binding is through protonated amine group of oleylamine. Figure 3.4 summarises the reaction scheme and adsorption mechanism.

3.I.3-1 Phase transfer of Hydrophobic γ-Fe_2O_3 nanoparticle of molar ratio 1:1 of Oa:Oam

The FeA nanoparticle was successully phase transferred using TMAOH and CTAB.[24(c,d)] Further through stober process silica coating was done over the surface of nanoparticle.[24c] The FTIR data in figure 3.4 clearly indicates the presence intense band at around 1100 cm^{-1}, which arises due to the siloxane bonds in curve (a) and (b). The protonated amines ($R_4N^{+)}$ of both CTAB and TMAOH is clearly seen in the figure 3.4. Work is in progress for further characterization of water dispersible γ-Fe_2O_3 nanoparticle.

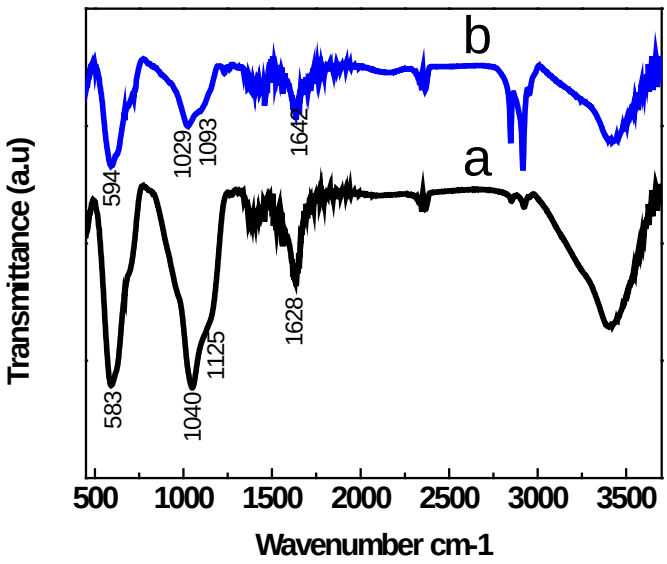

Figure 3.4: FTIR spectra of FeA phase transfered using (a) TMAOH and (b) CTAB

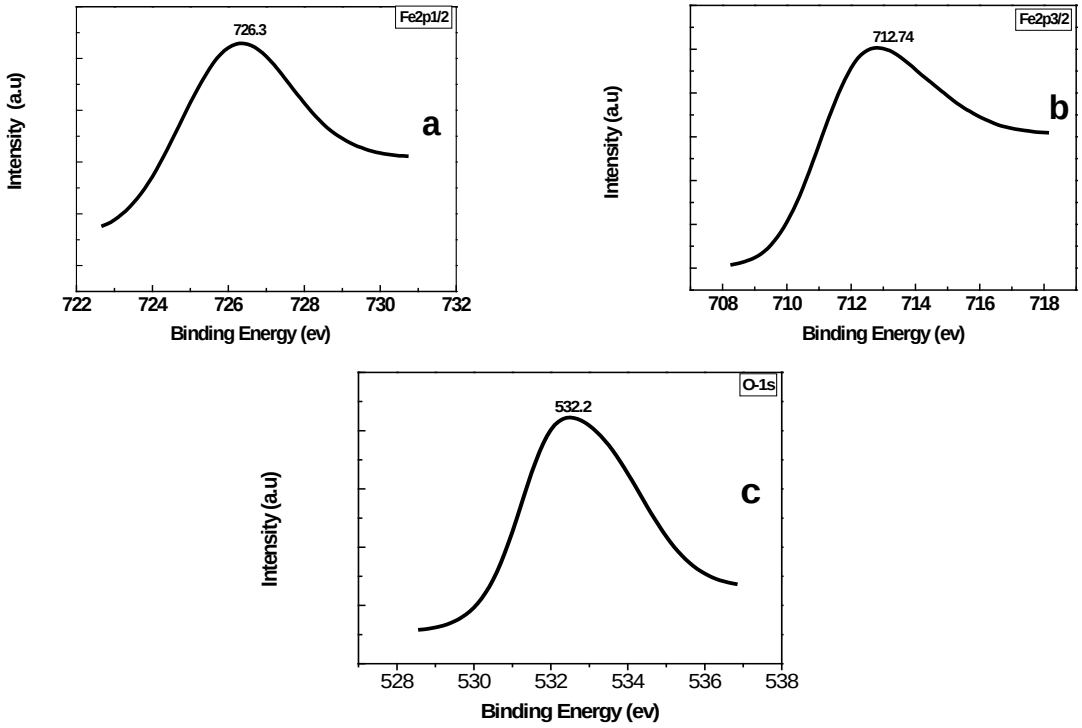

Figure 3.5: XPS spectra of FeA (a) $Fe2p_{(1/2)}$ (b) $Fe2p_{(3/2)}$ and (c) O1s

Figure 3.5 represents X-ray photoelectron spectrum of FeA γ-Fe_2O_3 nanoparticles. Characteristic doublet of $Fe2p_{3/2}$ and $2p_{1/2}$ core-level spectra at 726.3 and 712.74 ev respectively show the formation of γ-Fe_2O_3 phase. Corresponding O(1s) peak at 532.2 eV and Fe(2p) results are comparable to the reported values of γ-Fe_2O_3.[25]

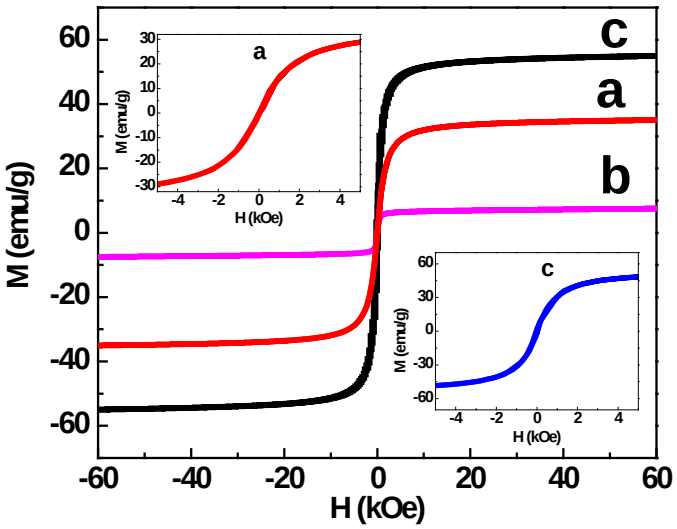

Figure 3.6 Field-dependent magnetization of (a) FeA,(b)FeBand(c) FeC

Figure 3.6 illustrates the magnetic properties of the nanoparticles, investigated with a quantum design physical property measurement system (PPMS). For the γ-Fe_2O_3 nanoparticles , the magnetization does not saturate, even for the applied field of 20 kOe and no hysteresis is observed. The M-H characterstics are typical of superparamagnetic behavior for all the magnetic nanoparticles (see inset figure 3.6). The estimates of the room-temperature saturation magnetization (Ms) value for these samples are obtained by the extrapolation of M versus 1/H curves to the limit 1/H curves to the limit 1/H 0 . The room temperature saturation magnetization values obtained are 34.5 emu/g, 6.65 emu/g and 49 emu/g respectively for FeA, FeB and FeC nanoparticles. The saturation magnetization values of these nanoparticls is less than the bulk values (80-85 emu/g) of γ-Fe_2O_3. A substantial decrease in the saturation magnetization value is attributed to the reduced particle size and to the existence of organic coating on the surface of nanocrystals. [26] The possible explanation could be due to the strong pinning of surface spins resulting in reduced exchange interactions.

SECTION II: Tuning Surface Functionalities of Superparamagnetic γ-Fe_2O_3 nanoparticles in view of Biomedical applications

In the present section, we report a one pot reaction to achieve water dispersible γ-Fe_2O_3 nanoparticles. In one pot reaction, NMP is chosen as both solvent and surfactant due to its coordination capacity with oxide and high boiling point. The nanoparticle were systematically functionalized by utilizing different surfactants as mentioned in Table 3.2. The amine functionalized magnetic nanoparticles enable covalent conjugation of fluorescein dye FITC by a modified protocol. [27]

We first prepared APTES-FITC, its –COOH group was subsequently amide bonded with free amine group in Fe-AM under basic condition using coupling agent EDC and NHS.

Table 3.2 Sample code, surfactant , TEM particle size and XRD crystallite size

Sample code	Surfactant	TEM particle size (±0.2nm)	XRD crystallite size (±0.5nm)
Fe-NMP	NMP	9	9
Fe-PEG	PEG	8	8
Fe-APT	APTES	5	5
Fe-AM	11-AM	4	4

3-I.1 RESULTS AND DISCUSSION

Figure 3.7 shows the representative TEM images of γ-Fe_2O_3 nanoparticles synthesized by different surfactants. Analysis of TEM micrographs clearly indicate the formation of monodispersed spherical nanoparticles for FeAM. Whereas Fe-NMP, Fe-PEG, and Fe-APT show the formation of irregular shaped particles. Particle size distribution anaylsis shows narrow size distribution for Fe-AM with mean particle size of 4 ± 0.2 nm. On the other hand Fe-NMP, Fe-PEG, and Fe-APT show wide particle size distribution. The lattic fringe analysis of Fe-APT and Fe-AM sample is included as the inset in figure 3.1 (c) and (d) respectively with d-spacing .

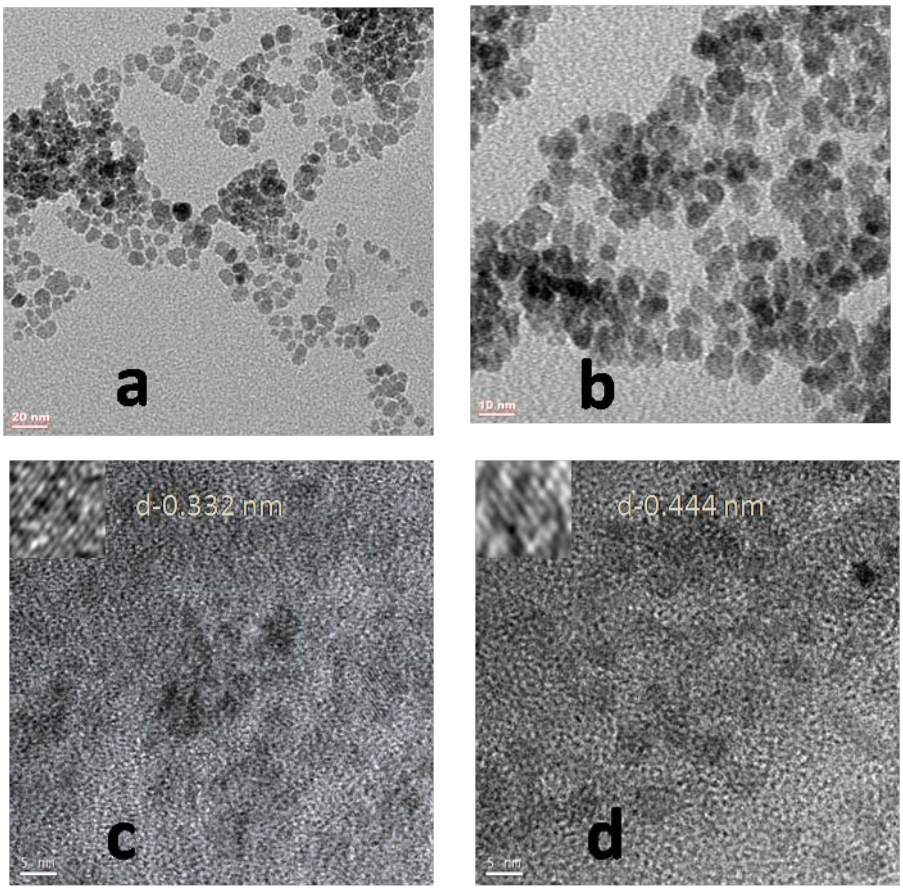

Figure 3.7: TEM images of (a) Fe-NMP, (b) Fe-PEG, (c) Fe-APT and (d) Fe-AM. Insets (c) and (d) corresponds to lattice fringes from HRTEM analysis

Figure 3.8 show powder x-ray diffraction patterns of γ-Fe_2O_3 nanoparticles. The XRD peak positions and relative intensities matches well with the JCPDS standard [39-1346]. The average crystallite sizes were calculated using scherrer formula. XRD crystallite sizes and TEM particle sizes are shown in Table 3.2 for comparsion.

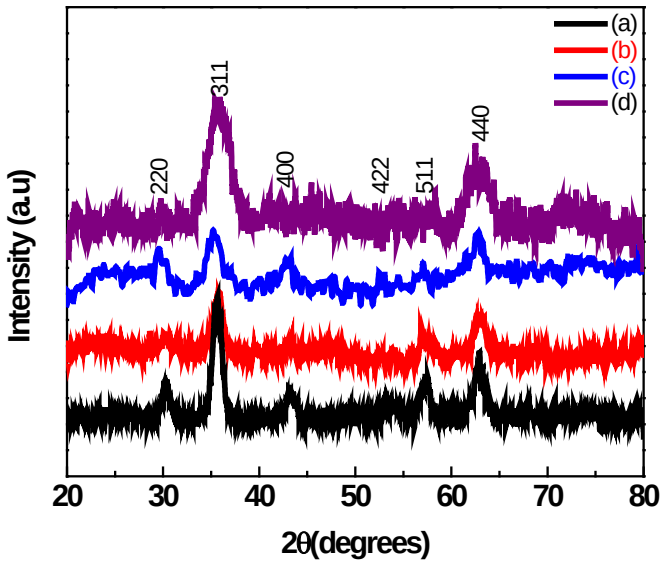

Figure 3.8: XRD pattern of (a) Fe-NMP (b) Fe-PEG, (c) Fe-APT and (d) Fe-AM

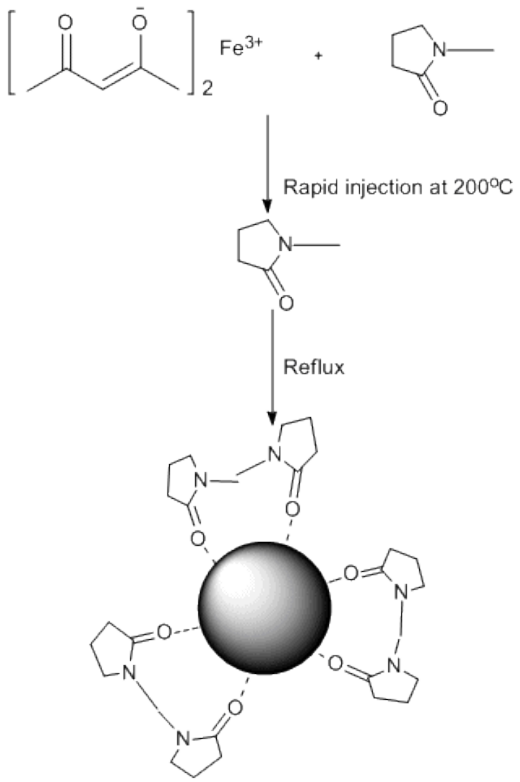

Schemel 1 : Reaction scheme and adsorption mechanism of NMP over surface of Fe-NMP

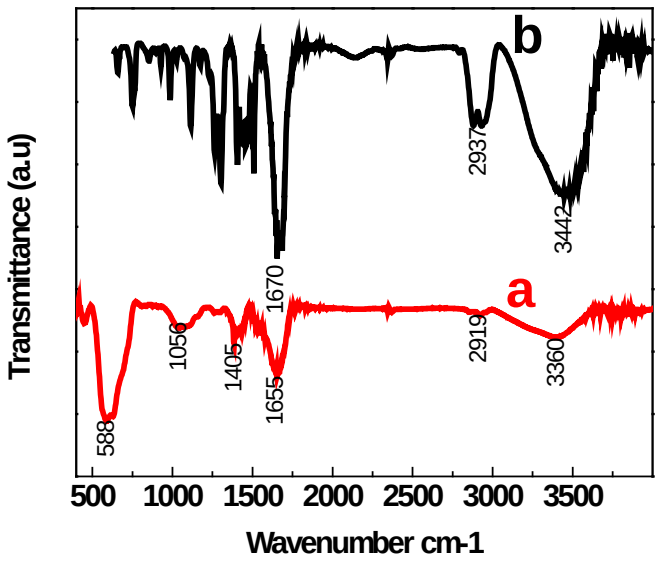

Figure 3.9: FTIR spectra of (a) Fe-NMP and (b) NMP

Figure 3.9 illustrates the FTIR spectra of the γ-Fe_2O_3 nanoparticles with both NMP as solvent and surfactant. FTIR spectra of Fe-NMP is composed with NMP vibrational bands. The FTIR measurements clearly reveal that the vibrational band of Carbonyl (C=O) shifts from 1679 cm- to 1655 cm^{-1}, indicating that the O from C=O coordinates on the surface of γ-Fe_2O_3 nanoparticles. A characteristic peak at around 588 cm^{-1} clearly indicates the formation of γ-Fe_2O_3. To understand further the adsorption of NMP over surface of the particle, TGA shown in figure 3.10 was analysed to calculate the thickness of the adsorped NMP which approximates to 1.39 nm and $9.1x10^{-5}$ NMP molecules per nanoparticle. The mass loss of 9% NMP bound to the surface of nanoparticle is attributed between 245ºC to 395ºC . Scheme 1 summarises the reaction scheme and adsorption mechanism.

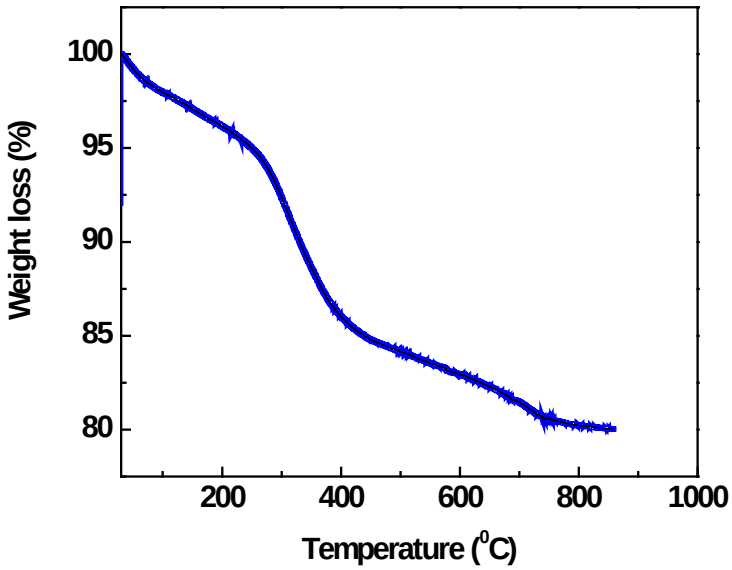

Figure 3.10: TGA of Fe-NMP

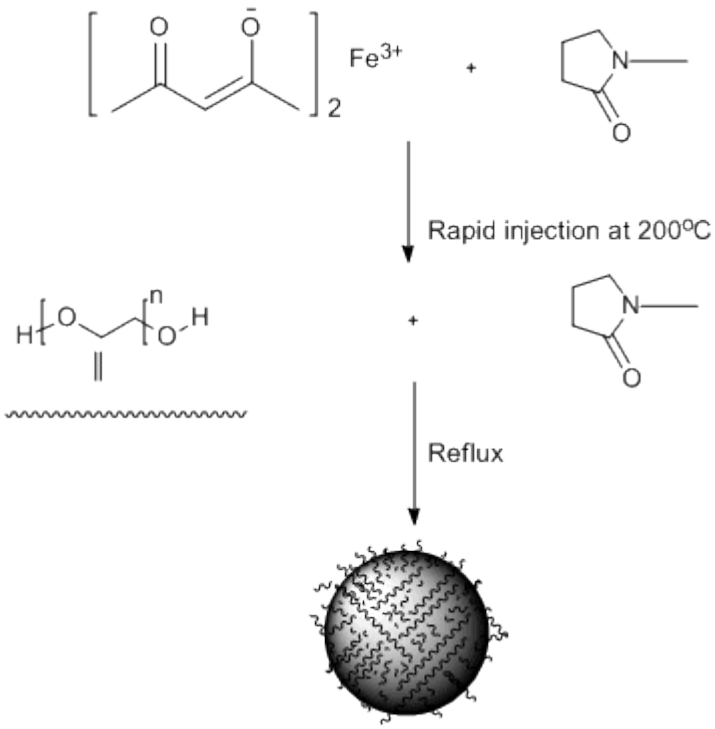

Scheme 2 : Reaction scheme and adsorption mechanism of PEG over surface of Fe-PEG

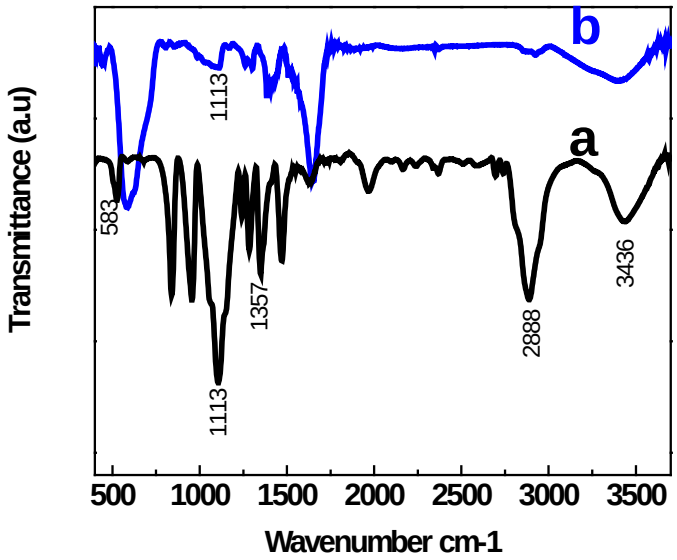

Figure 3.11: FTIR spectra of (a) PEG and (b) Fe-PEG

PEG covered γ-Fe_2O_3 nanoparticle has the advantage to inhibit the plasma coating and escape from the reticular-endothelial system (RES), like macrophage cells for longer circulation times in vivo application.[28(a,b,c)] Hence we have chosen functionalizing the nanoparticle with PEG. FTIR spectra of Fe-PEG is comparaed with PEG in figure 3.11. In the case of PEG-wrapped γ-Fe_2O_3 nanoparticle, the C–O–C symmetric stretch band at 1115 cm^{-1} and the vibration band at 1357 cm^{-1} (antisymmetric stretch) appeared in the FT-IR spectrum of the nanoparticles after surface modification. Similarly, the bands around 2888 and 961 cm^{-1}corresponded to –CH stretching vibrations and –CH out-of-plane bending vibrations, respectively. The C–O–C, −CH, and −CH peaks were strong evidence that PEG covered at the nanoparticle surface.[29,30a] To understand further the binding of PEG over surface of the particle, TGA shown in figure 3.12 was analysed to calculate the thickness of the adsorped PEG which approximates to 1.2 nm with 76 PEG polymer units per nanoparticle. The region chosen for PEG loss is from 241ºC to 405ºC attributed to mass loss of 11.4% of PEG as reported in similar kind of TGA profile for PEG coated ironoxide nanoparticle. [30(b,c)] Scheme 2 summarises the reaction scheme and adsorption mechanism.

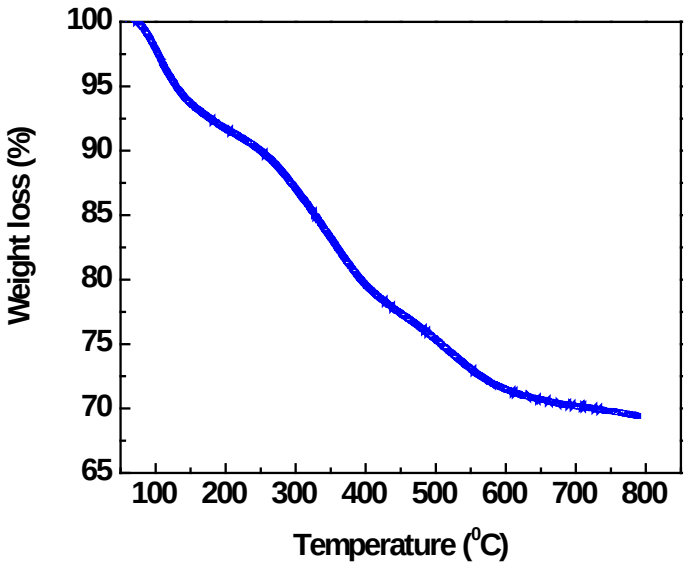

Figure 3.12: TGA of Fe-PEG

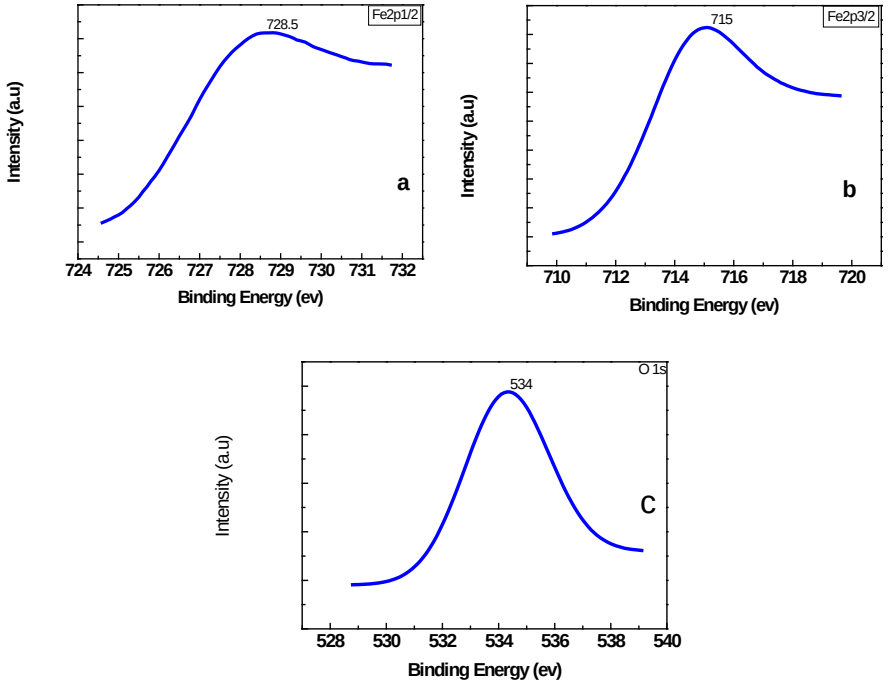

Figure 3.13: XPS spectra of Fe-PEG (a) $Fe2p_{(1/2)}$ (b) $Fe2p_{(3/2)}$ and (c) O1s

In order to further confirm the surface coordination and phase, x-ray photoelectronspecroscopy (XPS) analysis was performed. Figure 3.13 represents X-ray photoelectron spectrum of FeA γ-Fe_2O_3 nanoparticle. Characteristic doublet of $Fe2p_{3/2}$ and $2p_{1/2}$ core-level spectra at 728.5 and 715 ev respectively show the formation of γ-Fe_2O_3 phase. Corresponding O(1s) peak at 534 eV and Fe(2p) results are comparable to the reported values of γ-Fe_2O_3.[25]

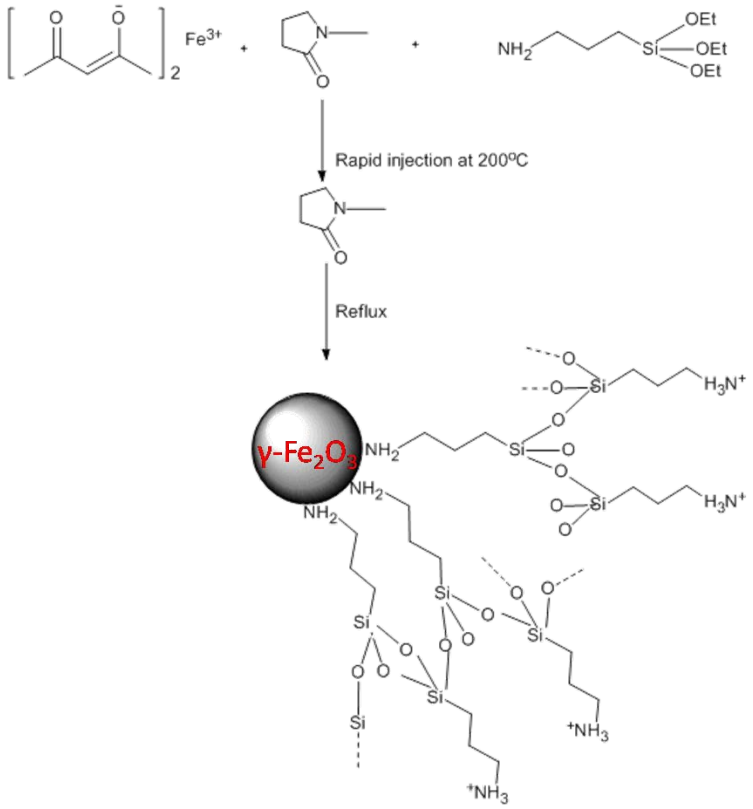

Scheme 3 : Reaction scheme and adsorption mechanism of APTES over surface of Fe-APT

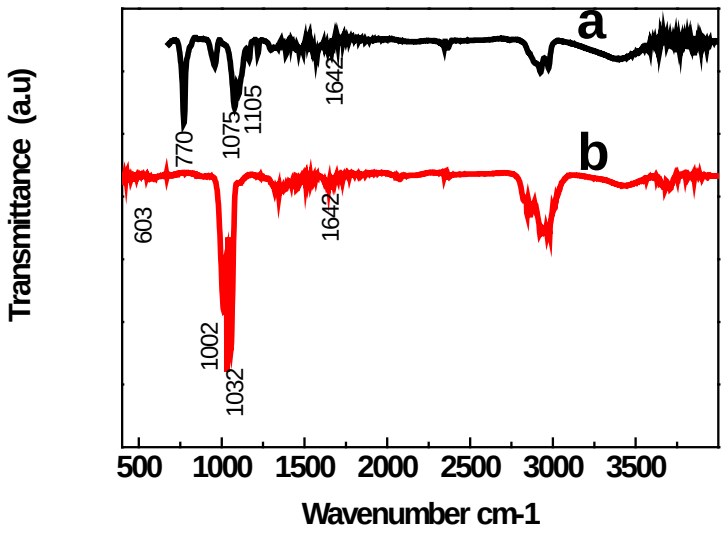

Figure 3.14: FTIR spectra of (a) APTES and (b) Fe-APT

In general, for biomedical applications of the magnetic nanoparticles, the surface has to be modified with amines, carboxyl etc. groups which enables covalent modification of the particle surface. Figure 3.14 clearly illustrates the capping of APTES on the surface of nanoparticle as indicated by presence of the intense band at 1100 cm^{-1}, which arises due to the siloxane bonds in curve (a) and (b). A weak broad absorption peak around 1642 cm^{-1} could be attributed to that of the antisymmetric deformation of the NH_3^+ group which may display the presence of the protonated amines. [20a] This protonated amines is present in surface of particle as indicated by figure 3.15 of zeta potential measurement with zeta potential of 37.8 mv. This possibly indicates that inially NH_2 group of APTES attach to the surface of nanoparticle subsequently there is condensation with another APTES molecule leading to protonated amine supported by FTIR data and positve zeta potential. Scheme 3 summarises the reaction scheme and adsorption mechanism.

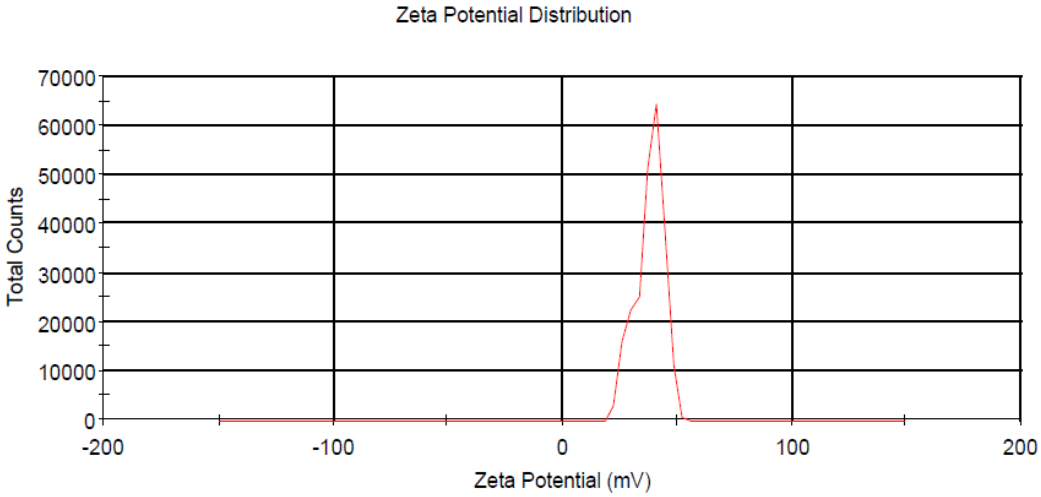

Figure 3.15: Zeta Potential of Fe-APT

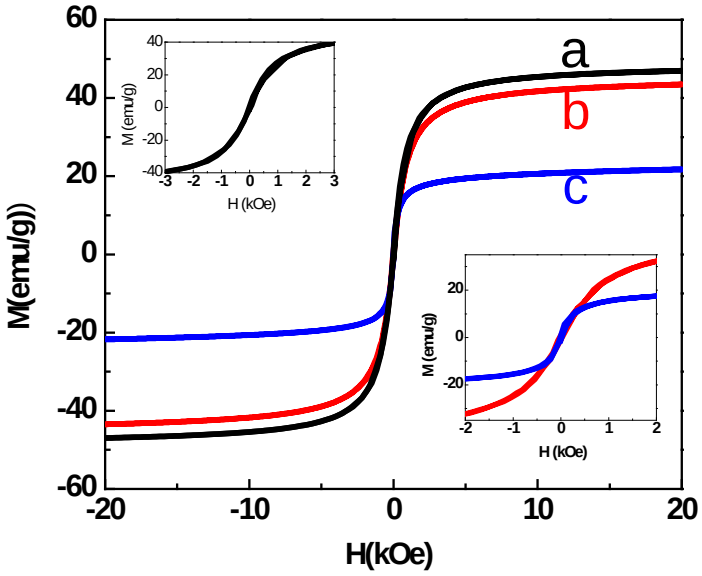

Figure 3.16: Field-dependent magnetization behavior of (a) Fe-NMP, (b) Fe-PEG and (c) Fe-APT

Figure 3.16 illustrates the magnetic properties of the nanoparticles, investigated with a quantum design physical property measurement system (PPMS). For the γ-Fe_2O_3 nanoparticles , the magnetization does not saturate, even for the applied field of 20 kOe and no hysteresis is observed. The M-H characterstics are typical of superparamagnetic behavior for all the magnetic nanoparticles (see inset in figure 3.16). The estimates of the room-temperature saturation magnetization (Ms) value for these samples are obtained by the extrapolation of M versus 1/H curves to the

limit 1/H curves to the limit 1/H → 0 . The room temperature saturation magnetization values obtained are 47.16 emu/g, 39.8 emu/g and 20.19.65 respectively for Fe-NMP, Fe-PEG and Fe-APT nanoparticles. The saturation magnetization of these nanoparticls is less than the bulk values (80-85 emu/g) of γ-Fe_2O_3. A substantial decrease in the saturation magnetization value is attributed to the reduced particle size and due to the existence of pinned surface spins. [26]

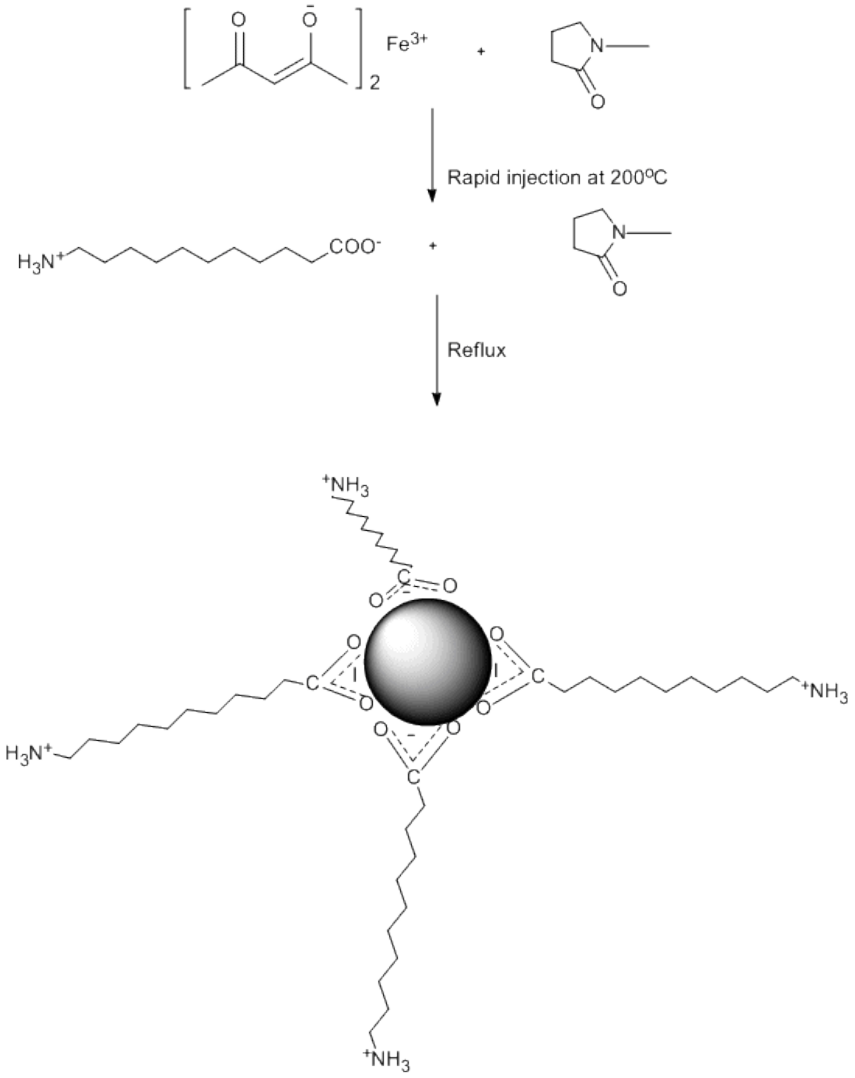

Scheme 4 : Reaction scheme and adsorption mechanism of 11-AM over surface of Fe-AM

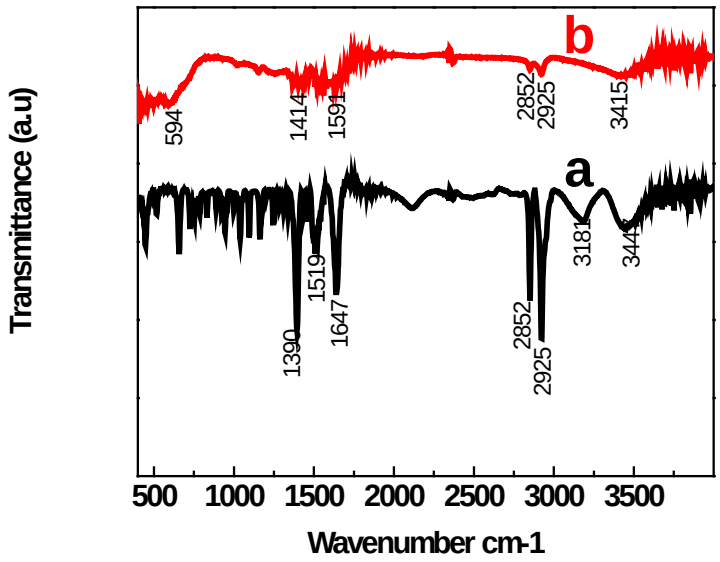

Figure 3.17: FTIR spectra of (a) 11-AM and (b) Fe-AM

Figure 3.17 clearly indicates the capping of 11-aminodecanioc acid on the surface of nanoparticle. . The peak at 1712 cm^{-1}, which is typical of the C=O stretch mode of the COOH group and the 3344 cm^{-1} symmetric stretching mode corresponding to the N-H stretch of NH_2 group are absent in curve (a) and (b) suggesting that the there is carboxylate anion and protonated amine. The carboxylatate anion binds to the surface of the nanoparticle and protonated amine hang on the surface as indicated by positve zeta potential of 9.15 mv in figure 3.18. Scheme 4 summarises the reaction scheme and adsorption mechanism.

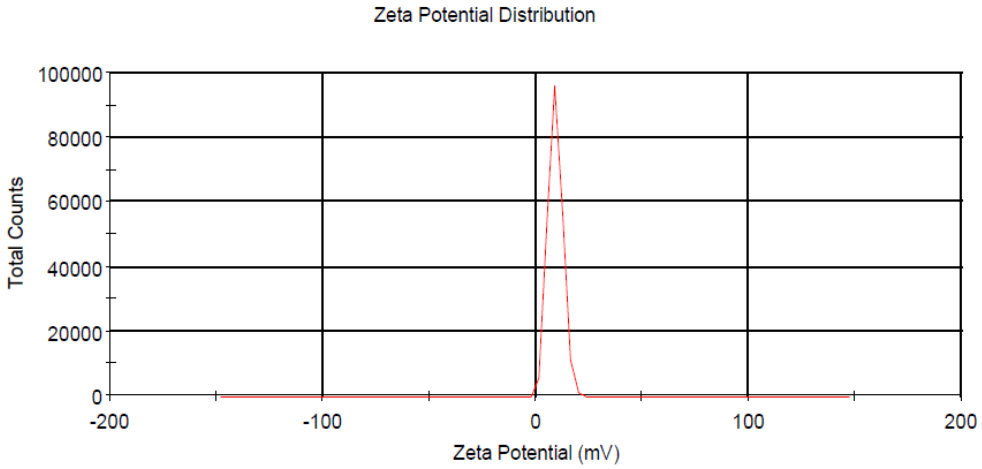

Figure 3.18: Zeta Potential of Fe-AM

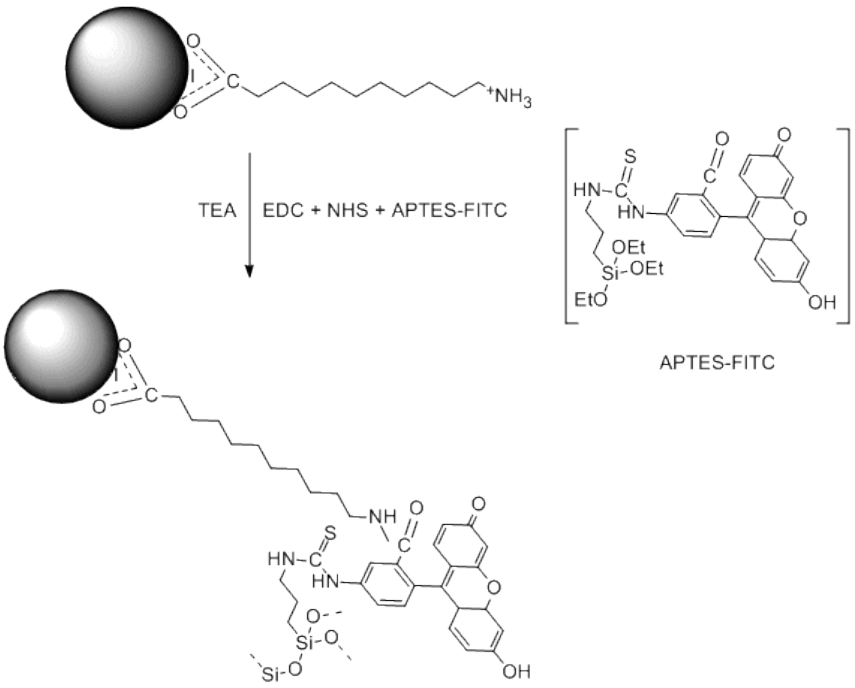

Scheme 5 : Reaction scheme for attachment of APTES-FITC with the surface of Fe-AM.

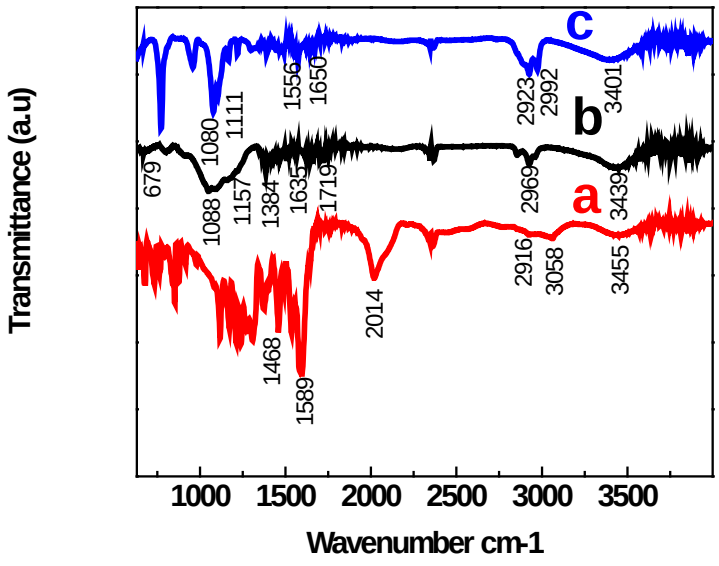

Figure 3.19: FTIR spectra of (a) FITC, (b) Attached APTES-FITC to Fe-AM and (c) APTES

Figure 3.19 clearly indicate the attachment of APTES-FITC to free amine group of γ-Fe_2O_3 nanoparticles through amide bond. The presence of the intense band at 1100 cm^{-1}, which arises due to the siloxane bonds in curve (b) and (c).

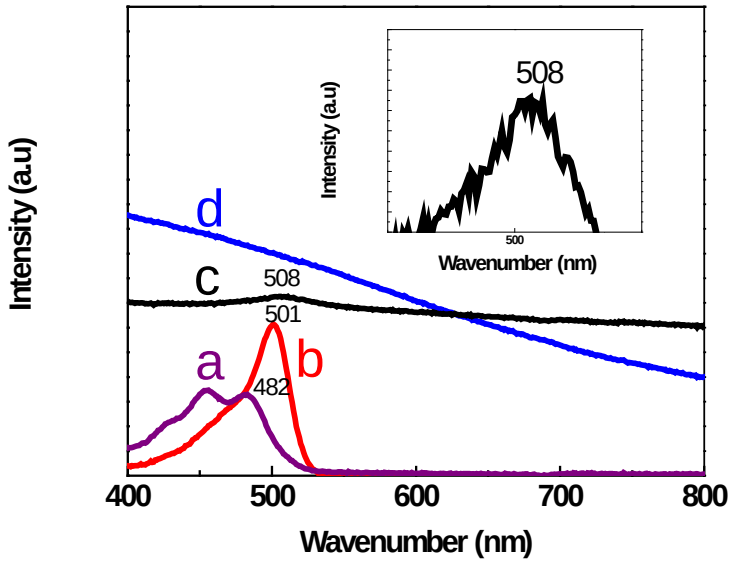

Figure 3.20: UV-VIS spectra of (a) FITC, (b) APTES-FITC, (c) Attached APTES-FITC to Fe-AM and (d) Fe-AM. Inset showing the absorption maximum of (c)

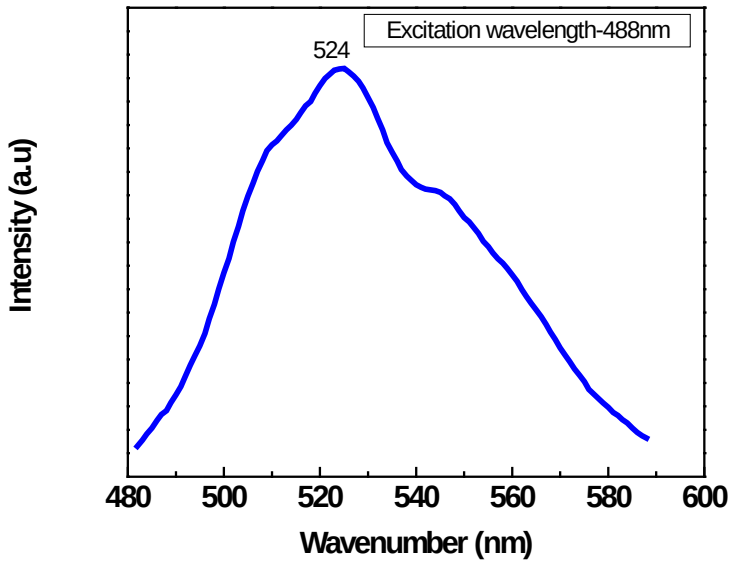

Figure 3.21: Photoluminescence (PL) spectra of Attached FITC to Fe-AM

The appearance of peak around 1630-1695 cm^{-1} corresponds to stretching vibration of C=O and 1590-1650 cm^{-1} corresponds to bending vibration of NH(Primary-amide), which is typically indicates the presence of amide bond, hence the attachment of APTES-FITC to surface of nanoparticle.[31]

Further UV-Visible spectra of figure 3.20 indicates the appearance of λmax at 508 nm in attached APTES-FITC to amine functionalized γ-Fe_2O_3 nanoparticles which is close to λmax at 501 nm of APTES-FITC in curve (b). The PL spectra as shown in figure 3.21 indicates the attached APTES-FITC to γ-Fe_2O_3 nanoparticles capped with 11-aminodecanoic acid shows fluorescence at 524 nm from the excitation wavelength at 488 nm. [24d,32] Scheme 5 summarises the reaction scheme and possible mechanism.

The present investigtions is in progress for encapsulating this fluoresscent magnetic nanoparticle in silica shells to provide a protective, biocompatible, inert, and hydrophillic surface with excellent anchoring points for derivatizing molecules.[33,34] Moreover, incorporation of chromophores in the silica shell provides magnetic and luminescent core/shell nanocomposites with applications as contrast agents for molecular imaging.[35,36]

3-III CONLUSIONS

In summary, this work demonstrates a simple strategy to achieve nearly monodispersed tunable surface functionalized γ-Fe_2O_3 nanoparticles by a modified thermal decompositon method utilizing a strong polar organic solvent, N methyl 2-Pyrrolidone (NMP) at much lower temperature 200ºC. The nearly monodispersed and spherical hydrophobic γ-Fe_2O_3 nanoparticles synthesized with equimolar ratio of oleic acid and oleyl amine can also be transferred to water and coated with silica shell, the characterization of these silica coated magnetic nanoparticle is in progress. As a result, we suggest that they are appropriate for biomedical applications, such as contrast agents for magnetic resonance imaging and drug delivery. We successfully presented a one step simple strategy to obtain water dispersible nearly monodispersed γ-Fe_2O_3 nanoparticles with surface functionalities utilizing NMP, Polyethylene glycol (PEG) of Mn 10,000, 3-Amino propyl Triethyl silicate (APTES) and 11-Aminodecanoic acid. The nearly monodispersed and spherical amine functionalized γ-Fe_2O_3 nanoparticle was further decorated with fluorescent FITC molecule to obtain stable water dispersible fluorescent magnetic nanoparticles, which can be further exploited for potential biomedical applications. The work in this direction is in progress.

3.IV REFERENCES

[1] Alivisatos, A P. Science 1996, 271(5251), 933-937.

[2] Huber, D. L Small 2005, 1(5), 482-501.

[3] Nelayah, J.; Kociak, M.; Stephan, O.; de Abajo, F.J.G.; Tence, M.; Henrard, L.; Taverna,D.; Pastoriza-Santos, I.; Liz-Marzan. L. M.; Colliexm, C. Nat. Phys. 2007, 3(5), 348-353.

[4] Batlle. X; Labarta. A J. Phys. D: Appl. Phys. 2002, 35(6), R5-R42.

[5] Murray, C. B.; Norris, D.j; Baendi. M; g. J. Am. Chem. Soc 1993, 115(19), 8706-8715.

[6] Roduner, E. Chem. Soc. Rev. 2006, 35(7), 583-592.

[7] Alivisatos, P. Nat. Biotechnoi. 2004, 22(1), 47-52.

[8] Tartaj. P.: Morales, M. P; Veintemillas-Verdaguer, S.; Gonzalez-Carreno. T.; Serna.C.J. J. Phys. D: Appl. Phys. 2003, 36(13), 15.

[9] Jun. Y. W.; Huh, Y.M.; Choi. J.S.;Lee J.H.; Song, H.T.; Kim, S.j.; Yoon. S.;Kim. K.S.: Shin, J. S.; Suh. J. S.; Cheon. J. J. Am. Chem. Soc. 2005. 127(16), 5732-5733.

[10] Yin. Y.; Alivisatos, A. P; Nature 2005, 4377(7059), 664-670.

[11] Park. J.; Lee, E.; Hwang, N. M.; Kang, M.; Sung, C. K.; Hwang, Y.; Park, J. G.; Noh, H. J.; Kim, J. Y.; Park, J. H.; Hyeon, T. Angew. Chem.. Int. Ed. 2005. 44(19), 2872-2877.

[12] Park. J.; An, K.; Hwang. Y.; Park, J.E.G.: Noh, H. J.; Kim, J. Y.; Park. J.H.; Hwang, N.M.; Hyeon, T. Nat. Mater. 2004, 3(12), 891-895.

[13] Sun.S.; Zeng, H. J. Am .Chem. Soc. 2002, 124(28), 8204-8205.

[14] Sun.S.; Zeng, H.; Robinson. D. B.; Raoux, S.; Rice. P.M.; Wang. S.X ; Li, G. J.Am. Chem. Soc. 2004, 126(1), 273-279.

[15] Guardia. P.; Batlle-Brugal, B.; Roca, A. G.; Iglesis, O.; Morales, M. P.; Serna, C.J.; Labarta, A.; Batlle, X. J. Magn. Mater. 2007, 316(2), E756-759.

[16] Roca. A.G.; Marco. J.F.; Morales, M. D.; Serna, C. J. J. Phys. Chem. C 2007, 111(50), 18577-18584.

[17] (a) Wu, N.; Fu, L.; Su, M.; Aslam, M.; Wong, K. C.; Dravid, V. P. Nano Lett. 2004, 4, 383. (b) Zhang, L.; He, R.; Gu, H-C. Appl. Surf. Sci. 2006, 253, 2611. (c) Guardia, P.; Battle-Brugal, B.; Roca, A. G.; Iglesias, O.; Marales, M. P.; Serna, C. J.; Labarta, A.; Battle, X. J. Magn. Magn. Mater. 2007, 316, e756. (d) Kataby, G.; Cojocark, M.; Prozorov, R.; Gedanken, A. Langmuir 1999, 15, 1703.

[18] Xu, Z.; Shen C.; Hou, Y.; Gao, H.; Sun, S. *Chem. Mater.* **2009**, *21*, 1778.

[19] (a) Sun, S.; Zeng, H. J. Am. Chem. Soc. 2002, 124, 8204. (b) Sun, S. Zeng, H.; Robinson, D. B.; Raoux, S.; Rice, P. M.; Wang, S. X.; Li, G. J. *Am. Chem. Soc.* **2004**, *126*, 273.

[20] Cannas, C.; Musinu, A.; Ardu, A.; Orru, F.; Peddis, D.; Casu, M.; Sanna, R.; Angius, F.; Diaz, G.; Piccaluga, G. *Chem. Mater.* **2010**, *22*, 3353.

[21] International Center for Diffraction Data, 12 Campus Boulevard, Newton Square, PA 39-1346.

[22] (a) H. Takey and S. Chiba, J. Phys. Soc. Jpn. 21, 1255 (1966). (b) Y. Kayanuma, Solid State Commun. 59, 405 (1986); Phys. Rev. B 38, 9797 (1988). (c) M Hayashi, T. Iwano, H. Nasu, K. Kamiya, N. Sugimotom and K. Hirao, J. Mater, Res. 12, 2552 (1997); B. Yu, C. Zhu, and F. Gan, Opt. Mater. 7, 15 (1997). (d) J. K. Vassiliou, V. Mehrotra, M. W. Russell, E. M. Giannelis, R. D. McMichael, R.D. Shull, andR. F. Ziolo, J. Appl. Phys. 73, 5109 (1993).

[23] Bu, W.; Chen, Z.; Chen, F.; Shi, J. *J. Phys. Chem. C*, **2009**, *113*, 12176.

[24] (a) Ren,Y.; Limura, K-I.; Kato, T. *Langmuir*, **2001**, *17*, 2688.(b) Jeng, J-Y.; Liu J-C.; Jean, J-H. *J. Am. Ceram. Soc*., **2007**, *90*, 3676. (c) Pablo Guardio, Nicolas Perez, Amilcar Labarta, and Xavier Batle Langmuir XXXX,XXX(XX), XXX- XXX. (d) Yu-Shen Lin and Christy L. Haynes Chem. Mater. 2009, 21, 3979-3986 .

[25] Cornell, R. M.; Schwertmann, U. *The Iron Oxides: Structure,Properties, Reactions, Occurrence and Uses*; VCH: Weinheim, 1996.

[26] Berkowitz, A. E.; Lahut, J. A.; Jacobs, I. S.; Levinson, L. M.; Forester, D. W. *Phys. Rev. Lett.* **1975**, *34*, 594.

[27] Ali Abou-Hassan, Rana Bazzi, and Valerie Cabuil Angew Chem. Int. Ed. 2009, 48, 7180-7183.

[28] (a) C. C. Berry, A. S. G. Curtis, *J. Phys. D. Appl. Phys.* **2003**, *36*, R198.(b) S. M. Moghimi, A. C. Hunter, J. C. Murray, *Pharm. Rev.* **2001**, *53*, (c) N. Kohler, C. Sun, A. Fichtenholtz, J. Gunn, C. Fang, M. Q. Zhang, *Small* **2006**, *2*, 785.

[29] Jin Xie, Chenjie Xu, Nathan Kohler, Yanglong Hou, and Shouheng Sun *Adv. Mater.* **2007**, *19*, 3163–3166

[30] (a) Chen Yue-Jian, Tao juan, Xiong Fei, Zhu Jia-Bi, Gu Ning, Zhang Yi-Hua, Ding Ye and Ge Liang *Drug Development and Industrial Pharmacy*, 2010; 36(10): 1235–1244 (b) Jinho Park, Mi Kyung Yu, Yong Yeon Jeong, Jin Woong Kim, Kwangyeol Lee, Vu Ngoc Phancand Sangyong Jon J. Mater. Chem., 2009, 19, 6412–6417 (c) Dongfang Liu, Wei Wu, Jingjing Ling, Song Wen, Ning Gu,* and Xizhi Zhang *Adv. Funct. Mater.* **2011**, *XX*, 1–7

[31] Introduction to Spectroscopy by Donald L.(Donald L. Pavia) Pavia (Author), Gary M. Lampman (Author), George S. Kriz (Author), James A. Vyvyan

[32] Ji Eun Lee, Nohyun Lee, Hyoungshu Kim, Jaeyun Kim, Seung Hong Choi, Jeong Hyun Kim, Taeho Kim, In Chan Song, Seung Pyo Park, Woo Kyung Moon, and Taeghwan Hyeon. J. AM. CHEM. SOC. 2010, 132, 552-557.

[33] M Stjerndahl, M. Andersson, H. E. Hall, D.M. Pajerowski, M. W. Meisel, R. S. Duran, Langmuir 2008, 24, 3532-3536.

[34] P. Sharma, S. Brown, G. Walter, S. Santra, B. Moudgil, Adv. Colloid Interface Sci. 2006, 471, 123-126.

[35] N. Insin J. B Tracy, H. Lee, J. P. Zimmer, R.M. Weservelt, M.G Bawendi, ACS Nano 2008, 2, 197-202.

[36] W.J.M Mulder, R. Koole, R. J Brandwijk, G. Storm¸ P.T.K Chin, G.J. Strijkers, C.D.M Donega, K. Nicolay, A. W. Griffioen, Nano Lett. 2006, 6, 1- 6.